REPORT DOCUMENTATION PAGE

Form Approved
OMB No. 0704-0188

1. REPORT DATE *(DD-MM-YYYY)*	**2. REPORT TYPE**	**3. DATES COVERED** *(From - To)*
June 2015	Journal Article	

4. TITLE AND SUBTITLE
Analysis of Self-Excited Combustion Instabilities Using Decomposition Techniques (Post-Print)

5a. CONTRACT NUMBER

5b. GRANT NUMBER

5c. PROGRAM ELEMENT NUMBER

6. AUTHOR(S)
Cheng Huang; William E. Anderson (Purdue University);
Matthew E. Harvazinski; Venkateswaran Sankaran (AFRL)

5d. PROJECT NUMBER

5e. TASK NUMBER

5f. WORK UNIT NUMBER
Q12J

7. PERFORMING ORGANIZATION NAME(S) AND ADDRESS(ES)

Air Force Research Laboratory (AFMC)
AFRL/RQR
5 Pollux Drive
Edwards AFB, CA 93524

8. PERFORMING ORGANIZATION REPORT NO.

9. SPONSORING / MONITORING AGENCY NAME(S) AND ADDRESS(ES)

Air Force Research Laboratory (AFMC)
AFRL/RQR
5 Pollux Drive
Edwards AFB, CA

10. SPONSOR/MONITOR'S ACRONYM(S)

11. SPONSOR/MONITOR'S REPORT NUMBER(S)
AFRL-RQ-ED-JA-2015-269

12. DISTRIBUTION / AVAILABILITY STATEMENT
Approved for public release; distribution unlimited

13. SUPPLEMENTARY NOTES
Journal article published in the AIAA Journal, Vol. 54, Issue 9, Sep 2016.
PA Case Number: 15353; Clearance Date: 6/29/2015.

14. ABSTRACT

Proper orthogonal decomposition and dynamic mode decomposition are evaluated for the study of self-excited longitudinal combustion instabilities in laboratory-scaled single-element gas turbine and rocket combustors. Since each proper orthogonal decomposition mode comprises multiple frequencies, specific modes of the pressure and heat release are not related, which makes the analysis more qualitative and less efficient for identifying physical mechanisms. On the other hand, dynamic mode decomposition analysis generates a global frequency spectrum in which each mode corresponds to a specific discrete frequency so that different dynamics can be correlated. In addition, proper orthogonal decomposition results are found to be inaccurate when only a limited amount of spatial information is provided in contrast with dynamic mode decomposition results, which provide more reliable results.

Overall, dynamic mode decomposition analysis proves to be a robust and systematic method that can give consistent interpretations of the periodic physics underlying combustion instabilities.

15. SUBJECT TERMS

16. SECURITY CLASSIFICATION OF:			**17. LIMITATION OF ABSTRACT**	**18. NUMBER OF PAGES**	**19a. NAME OF RESPONSIBLE PERSON**
					N/A
a. REPORT	**b. ABSTRACT**	**c. THIS PAGE**	SAR	17	**19b. TELEPHONE NO** *(include area code)*
Unclassified	**Unclassified**	**Unclassified**			

Standard Form 298 (Rev. 8-98)
Prescribed by ANSI Std. 239.18

AIAA JOURNAL
Vol. 54, No. 9, September 2016

Analysis of Self-Excited Combustion Instabilities Using Decomposition Techniques

Cheng Huang* and William E. Anderson†
Purdue University, West Lafayette, Indiana 47907
and
Matthew E. Harvazinski‡ and Venkateswaran Sankaran§
U.S. Air Force Research Laboratory, Edwards Air Force Base, California 93524

DOI: 10.2514/1.J054557

Proper orthogonal decomposition and dynamic mode decomposition are evaluated for the study of self-excited longitudinal combustion instabilities in laboratory-scaled single-element gas turbine and rocket combustors. Since each proper orthogonal decomposition mode comprises multiple frequencies, specific modes of the pressure and heat release are not related, which makes the analysis more qualitative and less efficient for identifying physical mechanisms. On the other hand, dynamic mode decomposition analysis generates a global frequency spectrum in which each mode corresponds to a specific discrete frequency so that different dynamics can be correlated. In addition, proper orthogonal decomposition results are found to be inaccurate when only a limited amount of spatial information is provided in contrast with dynamic mode decomposition results, which provide more reliable results. Overall, dynamic mode decomposition analysis proves to be a robust and systematic method that can give consistent interpretations of the periodic physics underlying combustion instabilities.

Nomenclature

A	=	proper orthogonal decomposition matrix
$a(t)$	=	temporal mode
m	=	number of spatial points
N	=	number of temporal points
N_p	=	total number of decomposed modes
p	=	pressure, Pa
p_c	=	mean chamber pressure, Pa
q	=	heat-release rate, W
Σ	=	proper orthogonal decomposition singular value matrix
T	=	dynamic mode decomposition temporal modes matrix
U	=	proper orthogonal decomposition temporal modes matrix
V	=	proper orthogonal decomposition spatial modes matrix
V_1^N	=	dynamic mode decomposition matrix from first to Nth snapshots
$\mathbf{\Psi}$	=	dynamic mode decomposition spatial mode(s) vector
$\boldsymbol{y}$	=	dynamic mode decomposition temporal mode(s) vector
$z(x, t)$	=	target function for postprocessing
$\Phi(x)$	=	spatial mode

Subscript

k	=	mode number

Superscript

$'$	=	perturbation variables

I. Introduction

DATA processing techniques based on proper orthogonal decomposition (POD) and dynamic mode decomposition (DMD) are powerful and elegant methods that can be used to obtain a low-dimensional approximate description of a high-dimensional physical process. POD has been extensively employed in the study of turbulence primarily for cold flow due to the limitations of experimental measurements in terms of both temporal and spatial resolution [1–3]. POD can also be used to extract mode shapes and basis functions. Its application in combustion problems has received some attention recently [4–6]; it has been used to gain insight into flame dynamics. DMD is a newer technique that has not yet been extensively used for reacting flow analysis. Thus far, DMD has been used in the investigation of flowfield characteristics [7–9]. Motheau et al. [10] applied DMD in reacting flows to investigate mixed acoustic–entropy interactions in a gas turbine.

Combustion instabilities arise due to the coupling of specific acoustic modes in the combustor configuration with the dynamics of the combustion heat release. When these phenomena occur in phase for a specific acoustic mode frequency, there is usually a constructive amplification of the mode, resulting in the growth of the mode and instability. Understanding the coupling of these phenomena is not trivial, especially for complex configurations involving multiple physical interactions, and the use of decomposition techniques such as POD and DMD provides an attractive basis for such analysis. The overall objective of this paper is to explore the use of POD and DMD techniques for analyzing combustion instability data. In general, the source of the data may be from experiments or from computations, but the present analysis uses computational results for definiteness.

Traditional data processing in combustion instability analysis involves the bandpass filtering of the signals around a frequency of interest. The frequencies of interest can be determined from a power spectral density (PSD) analysis of the signal. In this way, the correlation between acoustics and combustion can be explored within a certain frequency range. However, filtered results are sensitive to several factors like filter type, bandwidth, and sample quality. One primary advantage of the decomposition techniques over filtering is that they work with the entire data set with minimal information loss.

Received 16 June 2015; revision received 19 December 2015; accepted for publication 4 May 2016; published online 5 July 2016.

*Postdoctoral Research Assistant, School of Aeronautics and Astronautics. Student Member AIAA.
†Professor, School of Aeronautics and Astronautics. Member AIAA.
‡Research Aerospace Engineer, Rocket Propulsion Division. Member AIAA.
§Senior Scientist, Rocket Propulsion Division. Senior Member AIAA.

Moreover, unlike filtering techniques, POD and DMD do not require prior knowledge or preanalysis of the data to obtain the dominant frequencies. Another motivation is that decomposition techniques are capable of extracting dynamically significant structures from the flowfield of interest. Each decomposed mode can be represented in terms of a spatial response and a temporal response, which provides detailed insight into the dynamics of acoustics and combustion.

In this paper, a lean direct injection (LDI) gas turbine combustor and a gas–gas coaxial rocket combustor are selected as two representative test configurations to explore the use of POD and DMD. The simulation of the single-element LDI combustor was performed by Huang et al. [11,12] and showed a low-level instability (p'/p_c within 5%). Couplings of acoustic and hydrodynamics modes are identified as important mechanisms that sustain instability in the combustor [12]. Related experimental studies of this combustor configuration were done by Gejji et al. [13]. Multiphysics and diverse frequency content were found in both experiment and computation. The simulation of the rocket combustor was performed by Harvazinski et al. [14,15] and showed a high-level instability (p'/p_c up to 35%). A distorted triple flame was found in a large-eddy simulation of the same geometry by Garby et al. [16] and Harvazinski et al. [17]. Experimental measurements of this configuration have been published previously, and recent results were given by Feldman et al. [18]. The present POD and DMD analyses are carried out using the aforementioned simulation data sets of Huang et al. and Harvazinski et al. The primary motivation of this study is to develop systematic approaches and techniques for the analysis of complex data sets that can be used for comparison, validation, and identifications of physical mechanisms. Specifically, we focus on the fundamental interactions between acoustic waves and unsteady combustion heat release and are interested in elucidating these effects at specific frequencies that may contribute to the generation of combustion instabilities. In addition, we also evaluate the capabilities of the methods to deal with data sets of different spatial extents and temporal resolution to determine their overall reliability for complex problems.

The remainder of the paper is organized as follows. In Sec. II, an overview of the two test cases [LDI and a continuously variable resonant combustor (CVRC)] with preliminary analysis of simulation results is presented. This helps to address difficulties with traditional filtering techniques and also emphasizes the importance of developing a systematic approach to study combustion instability. Section III is a comparison between POD and DMD results for the two test cases. The results demonstrate that DMD is the preferred approach for our applications. A summary of the comparisons and conclusions are given in Sec. IV. In addition, supplementary materials are provided in the Appendix with the mathematical details given in Appendix A for POD and DMD. We then consider more detailed performance evaluations of the DMD procedure in Appendix B.

II. Background

For many applications, raw data are available as a series of snapshots. The purpose of the decomposition is to take a collection of data snapshots and decompose it into a reduced form. In the case of POD, this decomposition is done using a singular value decomposition (SVD), while for DMD, the data are reduced using the Arnoldi algorithm. POD decomposes data based on optimality to obtain a set of best representations of the original data set. A detailed description of the POD method is given by Chatterjee [19] and Berkooz et al. [3]. DMD decomposes the data based on frequencies, and an introduction to this technique can be found by Rowley et al. [20] and Schmid [21]. Both POD and DMD result in decomposed modes. POD generates modes that are orthogonal in both space and time, while DMD generates decomposed modes based on discrete frequencies. A brief overview of the mathematical models of POD and DMD can be found in Appendix A.

A. Single-Element LDI Gas Turbine Combustor

A detailed description of the LDI gas turbine combustor can be found in [12,13]. The computational domain used for the simulations and decomposition analysis is shown in Fig. 1. Hot air ($T_{\text{air}} = 800$ K) enters through the air plenum and passes through a swirler just before the converging–diverging venturi shown in Fig. 1 (detail B). Air mixes and reacts with incoming liquid fuel (Jet A) quickly in the venturi section because of the presence of a strong swirling flow. The air plenum is 56 cm long, and the combustion chamber is 108 cm long. Choked slots (Fig. 1, detail A) and choked exit nozzle (Fig. 1 detail C) are used at the domain inlet and outlet, respectively, to enforce ideal acoustic boundary conditions for both experiment and simulation. The chamber is designed to sustain acoustics at fundamental frequency around 300 to 400 Hz with mean chamber pressure p_c at 1 MPa. Five million grid points are used for the simulation.

For this study, a low equivalence ratio ($\Phi = 0.36$) is selected for POD and DMD analysis due to the wide range of frequencies observed in both the experiment and simulation (see Fig. 2). Frequency

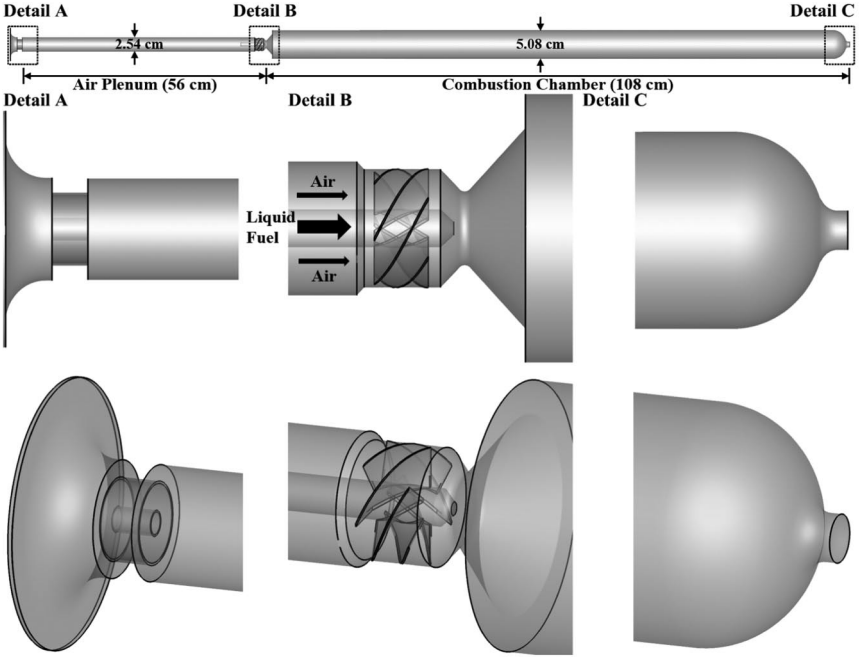

Fig. 1 LDI computational domain used for decomposition analysis.

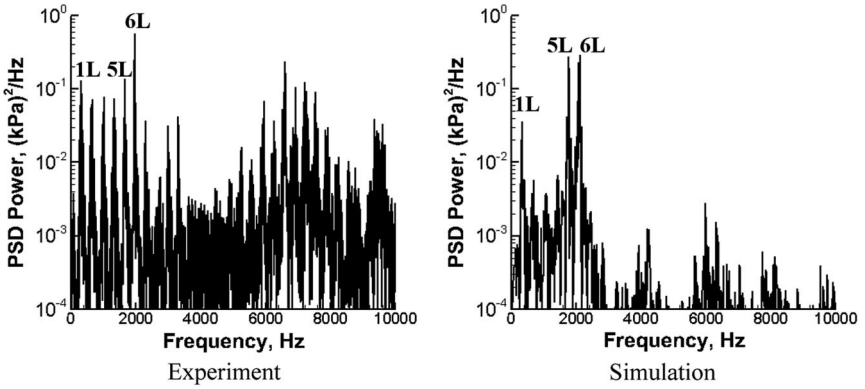

Fig. 2 PSD analysis for the experiment (left) and simulation (right) of LDI combustor (signals are taken 4.6 cm downstream to the exit of the venturi) [12].

content ranges from 330 to 8000 Hz. The fifth and sixth longitudinal modes are dominant in both the simulation and experiment. These two high-order acoustic harmonics couple with the natural hydrodynamic modes that exist in the combustor [12].

The time-averaged heat-release rate is shown in Fig. 3 with a black isoline of zero axial velocity ($U = 0$), used to indicate the vortex breakdown bubble, the interactions with acoustic field of which have been proposed to be the key mechanism to sustain combustion instability in this LDI combustor [12]. The majority of the heat release takes place in the diverging section of the venturi following the cone angle into the combustor surrounding the vortex breakdown bubble. Six locations in the chamber head section are selected to study the PSD analyses for the pressure and heat-release signals, which are shown in Figs. 4 and 5, respectively.

Interestingly, acoustic responses in this single-element LDI combustor show both local and nonlocal effects. The pressure signals show consistent dominance of 5L and 6L (L stands for longitudinal acoustic mode) frequencies consistent with Fig. 2 at all locations, but there are some differences in the high-frequency region (4 to 7 kHz), the responses of which are largely dependent on the location. As the flow moves downstream into the combustor, the high-frequency response is weakened.

The heat-release responses in Fig. 5 show greater dependence on locations. The dominance of the low frequency (1L and 2L etc.) are observed in the upstream location (point 1) close to the venturi throat, while downstream there is a greater dominance of high frequencies. The strongest acoustic mode, 6L, is still dominant in the heat-release responses at several locations, while at the outer edge of the cone (point 3), a higher frequency (~6 to 7 kHz) is dominant. The PSDs for

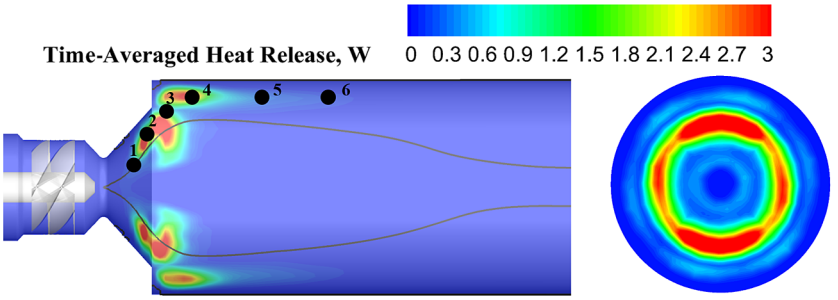

Fig. 3 Time-averaged heat-release rate contour of LDI simulation (black line: $U = 0$, indicating vortex breakdown bubble).

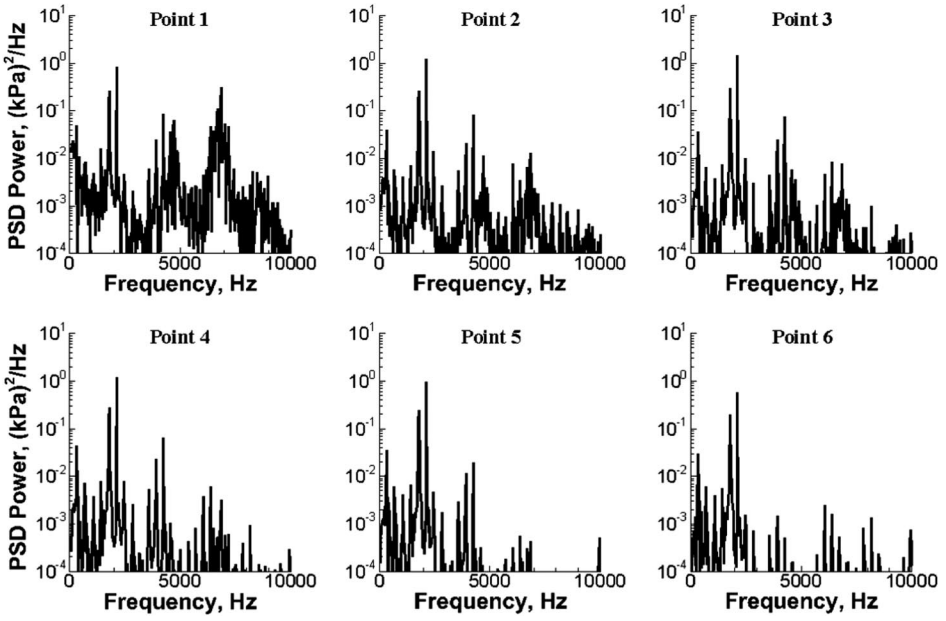

Fig. 4 PSD analysis for pressure signals at different locations (highlighted in Fig. 3) in LDI simulation.

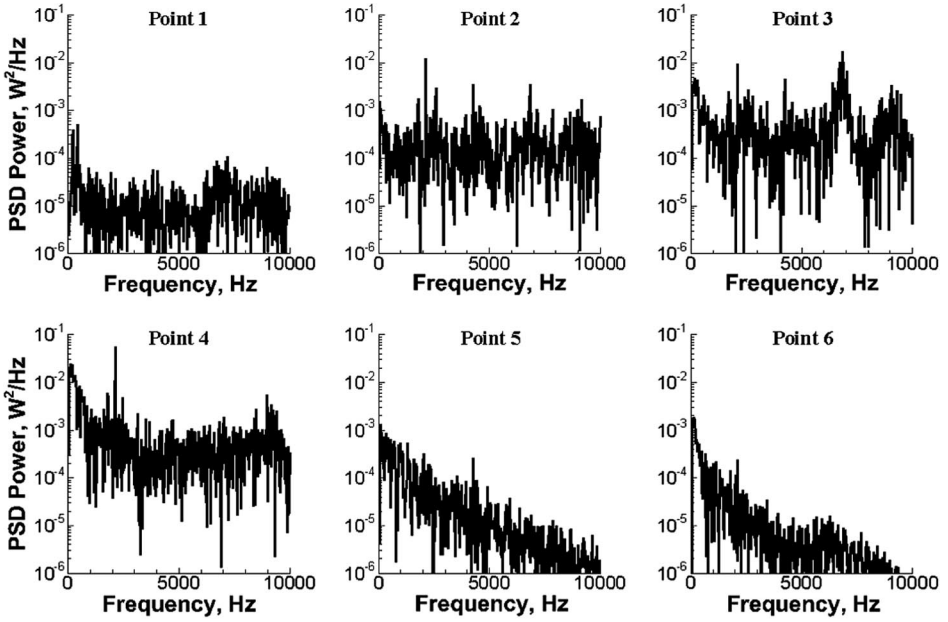

Fig. 5 PSD analysis for heat-release signals at different locations (highlighted in Fig. 3) in LDI simulation.

points 5 and 6 show less frequency content, which indicates that the mean heat-release responses are weak. Heat release is driven by mixing and chemistry, which are governed by local effects, unlike the pressure, which is mainly a global acoustic response. This increases the difficulties in investigating the coupling between local combustion and global acoustic responses in combustion instability studies and hence our interest in using POD and DMD analyses to probe such effects. In addition, the identification of mechanisms that promote higher acoustic harmonics and the local pressure fluctuations further require efficient postprocessing techniques.

B. CVRC Model Rocket Combustor

The rocket injector geometry used in the present study is the CVRC experiment, which has been modeled using Detached Eddy Simulation by Harvazinski et al. [14,15]. The experiment features a variable length oxidizer post, which produces varying levels of instability. For this simulation, a single operating point is considered. The domain used for the simulation and decomposition analysis is shown in in Fig. 6. The oxidizer is decomposed hydrogen peroxide and enters from the left through the oxidizer post. The fuel, gaseous methane, enters just before the backstep. For the simulation, the oxidizer post length is fixed at 13.97 cm. This represents an unstable operating point with a fundamental longitudinal acoustic frequency between 1300 to 1500 Hz and mean chamber pressure p_c at around 1.65 MPa.

Figure 7 shows the power spectral density results of the raw pressure signals from the computational and experimental results [15]. The first six strongest acoustic frequencies can be observed from the figure. The experimental results indicate lower values of frequencies compared with simulation results, but the higher modes are near integer multiples of the first mode [18].

An overview of combustion dynamics within a representative acoustic cycle is given in Fig. 8 for the CVRC simulation. The high-pass filtered pressure signal is monitored at the chamber head section, and four points in a 1L period are selected to identify the combustion response (a central slice is extracted to visualize heat-release and vorticity dynamics of the three-dimensional flowfield). The acoustics at the head section goes through a slow expansion (time 1 to 3) and a rapid compression (time 3 to 4). The combustion and flow dynamics follow the acoustics such that during expansion the vorticity level is decreasing, which slows down the mixing between the fuel and oxidizer, and therefore there is less heat release produced in the combustor, while as the acoustics moves into compression, the vorticity level starts to rise near the dump plane at time 3, which enhances the fuel–oxidizer mixing and consequently leads to a significant rise in the heat-release rate. Based on these investigations, qualitative understanding of the combustionacoustic coupling can be obtained. However, more quantitative and systematic postprocessing techniques are required to establish more precise correlations

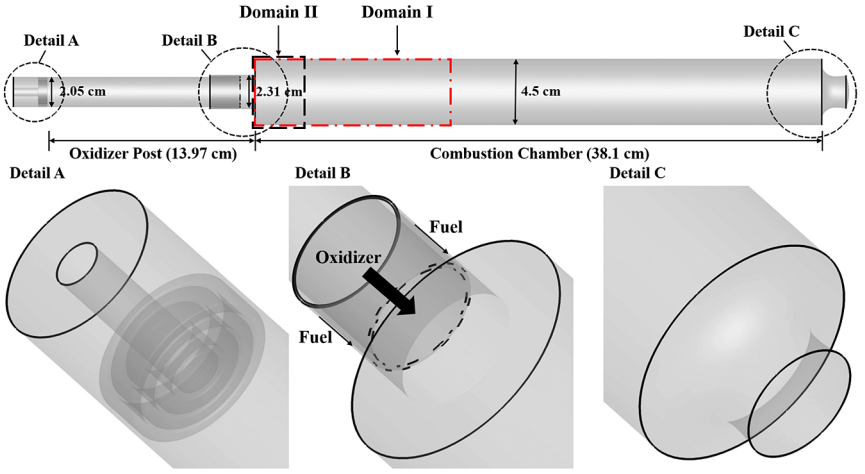

Fig. 6 CVRC computational domain showing the regions used for decomposition analysis (domain I is the combustion done, and domain II is one-quarter of domain I).

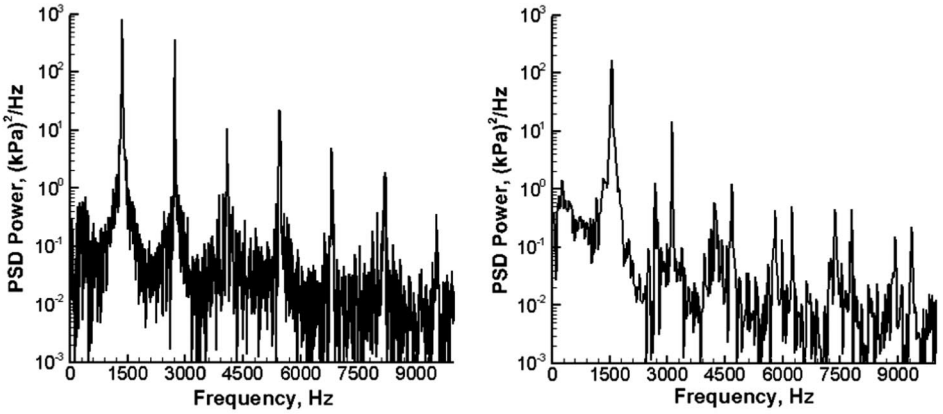

Fig. 7 PSD analysis for the experiment (left) and simulation (right) of CVRC [15].

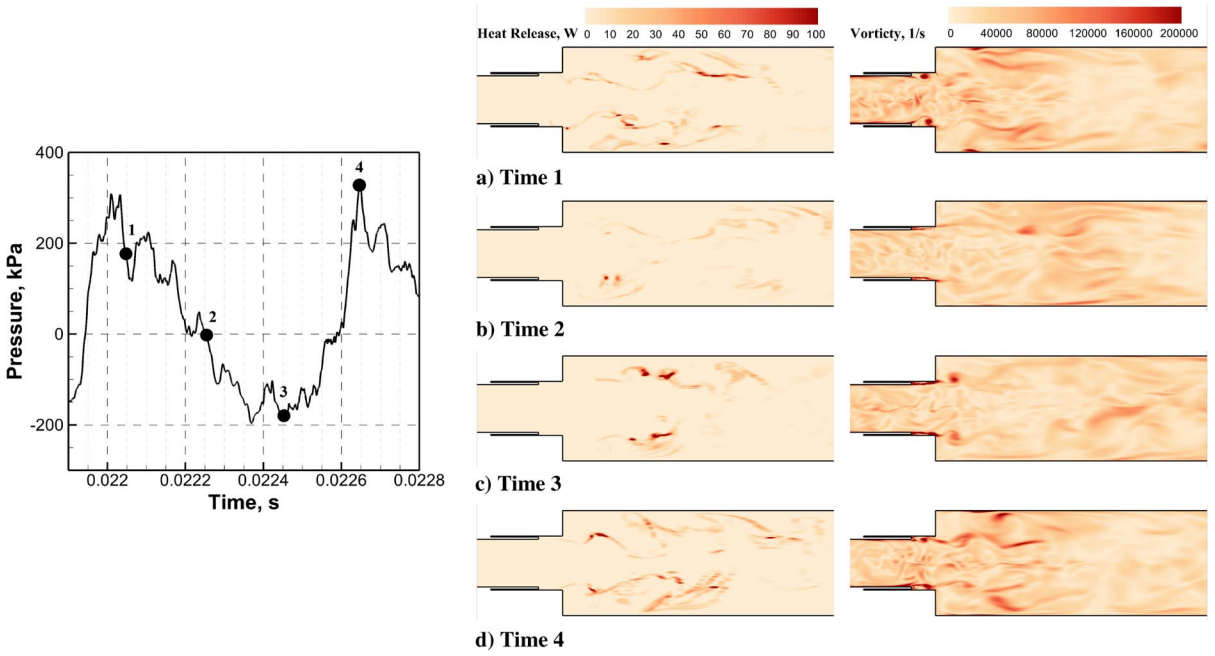

Fig. 8 Overview of cycle behavior of combustion and flow dynamics (right) with regard to pressure oscillations (left).

between certain acoustic modes and the combustion response. In addition, efficient tools are needed to extract more statistically stationary information from the highly unsteady and spontaneous flame behavior seen in Fig. 8.

III. Results

In this section, decomposition results are discussed with specific emphasis on comparing the POD and DMD methods in terms of capabilities for capturing the important dynamics of the p' and q' variables. For the LDI combustor, comparisons between POD and DMD are focused on the efficiency of each technique for providing useful information of acoustic and combustion dynamics. For the CVRC, studies focus on the capabilities of the techniques when dealing with incomplete information. Subdomains (dashed regions in Fig. 6) are used in addition to the full domain to evaluate the effect of incomplete information on the decomposition technique.

To study the unsteadiness of physics occurring during combustion instability, the mean values of the pressure and heat-release rate are subtracted from the raw data before the analysis for both combustors. Only the fluctuating portions of the pressure p' and heat-release rate q' are used. To reduce the amount of data for postprocessing, information is interpolated from the original fine computational grid to a coarser grid. This is needed due to the large memory requirement of the decomposition techniques and the large number of cells used for the CFD simulations.

Before proceeding to the rest of the results section, it is useful to compare the basic properties and capability of POD and DMD [22]. Given a sequence of snapshots from either experiment or simulation, POD decomposes the data set to maximize the inner product of the dynamics provided for an optimal representation of the original information (mathematical details are given in Appendix A1), while DMD calculates the temporal transition between snapshots to identify coherent structures corresponding to one single frequency (mathematical details are given in Appendix A2). In this respect, the temporal evolution for each POD mode may contain a range of frequencies, which might make it less efficient than DMD in dealing with temporally coherent problems (e.g., combustion instability). On the other hand, it should be pointed out that for analysis of transient problems that are lack of temporal coherence (e.g., laminar–turbulent transition), the energy-based POD approach might have more advantages over the frequency-based DMD approach.

A. Single-Element LDI Gas Turbine Combustor

1. *POD Analysis*

For the LDI, the entire geometry is used for decomposition analysis. The POD analysis decomposes the whole data set based on

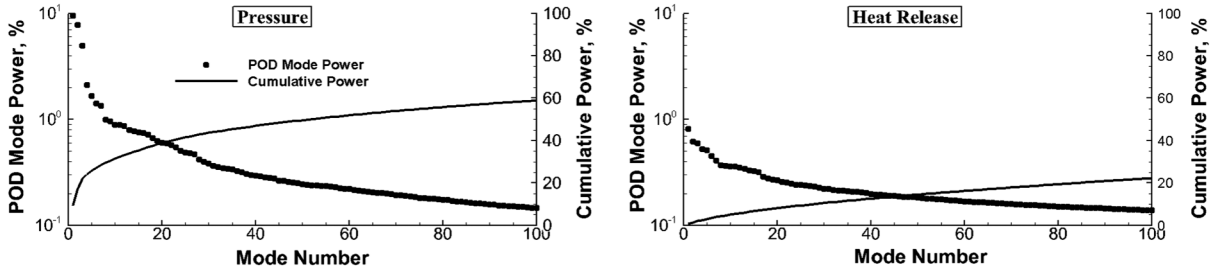

Fig. 9 POD mode power vs mode number for pressure (left) and heat-release (right) fluctuations in LDI combustor (POD mode power is plotted on a log scale).

the significance of single modes to minimize the error between the decomposed modes and the original data set. The POD mode power represents the weighting of each mode and is defined as the normalized singular value in Eqs. (A4) and (A5), while the cumulative power, defined as the summation of POD mode power, is useful for checking the reconstructed solution data. These quantities are defined as follows:

$$\text{POD mode power} = \frac{\sigma_i}{\sum_i \sigma_i} \times 100\%$$

$$\text{Cumulative power} = \frac{\sum_{i=1}^{k} \sigma_i}{\sum_i \sigma_i} \times 100\% \tag{1}$$

The POD mode power and cumulative power are plotted against the mode number in Fig. 9 for both the pressure and heat-release fluctuations. For the pressure, the first several modes contain a significant percent of the total power. After the first ten modes, there is a rapid decay in the mode power, indicating that nearly all of the required information to reconstruct the pressure mode can be found in the first few modes. For the heat release, on the other hand, there is a gradual decrease in mode power. The most dominant mode of heat release contains only 1% of the mode power compared to 10% in the case of pressure. To reconstruct the heat release, therefore, a significantly larger number of modes is required. By including the first 100 POD modes, 60% of the power of the pressure fluctuations and 20% of the power of the heat-release fluctuations are captured. The mode power summary suggests that for organized and periodic physics, like acoustics, only a few POD modes are needed to represent the response. For spontaneous and highly nonlinear physics, like combustion, a large number of POD modes is needed. When a large number of modes is required, the benefit of using a decomposition technique is minimized.

Four representative POD modes are selected for pressure and are shown in Fig. 10. A PSD analysis of the temporal signal of each POD mode shows which modes are present. A cross-sectional slice along with a single axial slice are used to visualize the spatial modes. For the heat release, the cross-sectional slice is restricted to the combustor head end, where most of the combustion takes place.

In each single POD mode, multiple frequencies are present. In the case of the pressure fluctuations, the 5L and 6L frequencies are dominant in POD modes 1 and 2. The side view shows a six half-wave configuration, while the axial view shows a uniform distribution. The global acoustic response of the system (Fig. 4) is captured by the lower POD modes, which contain the most energy. The nonstationary characteristics of the signals result in a zero-frequency mode showing up in POD modes 1 and 2.

Local acoustic responses are also observed in Fig. 4; these appear in the higher POD modes with a dominant frequency of 7000 Hz. This mode is related to the hydrodynamic precessing vortex core (PVC) mode [11,12]. Contributions from the 1L and 6L acoustic modes are still identifiable but are suppressed. The mode shape for POD modes 10 and 11 are different than the global mode shapes seen for POD modes 1 and 2. A weak response is found in the chamber section, while the venturi section (the zoomed-in area highlighted by the dashed rectangular box) shows elevated content, and the axial slice shows the contribution from the swirling motion of the flow and the PVC mode.

The first four heat-release modes are shown in Fig. 11. Frequencies observed in the POD results of pressure are also found in the heat release throughout the first four modes. Unlike the pressure, for which the modes with similar frequency content appear in neighboring modes, the 6L response is split between modes 1 and 4 for the heat release, while modes 3 and 4 are dominated by the higher frequencies present in modes 10 and 11 for pressure. Heat-release modes 1 and 4 show variations in the longitudinal direction and a uniform distribution in the azimuthal direction. On the other hand, identifiable azimuthal variations are found in heat-release modes 2 and 3 with strong indications of a spiral structure. Based on the frequencies and spatial mode shapes, pressure modes 1 and 2 can be correlated with heat-release modes 1 and 4, both revealing responses driven by longitudinal acoustic modes, and pressure modes 10 and 11 seem to be related to the heat-release modes 2 and 3, which contain the effects of the swirling flow.

In the LDI combustor simulation, the POD analysis is seen to be capable of capturing important mode shapes for both pressure and heat-release fluctuations at different frequencies. Qualitative understandings of the contributions from certain frequencies can be obtained from the spatial modes, and couplings between pressure and heat release can be partially addressed by establishing connections based on the dominant frequencies. However, POD analysis is not able to provide robust one-on-one correlations between pressure and heat-release modes. Though correlations can be established based on the PSD analysis of the temporal signals, the nonpairing of the responses makes it difficult to interpret the data and make specific connections. Moreover, any understanding that can be derived requires additional work that can be tedious and time consuming given the large number of frequencies of interest. Further, the presence of multiple frequencies in each POD mode also increases the difficulty of distinguishing the responses under different frequencies. For example, in heat-release modes 2 and 3 (Fig. 11), PSD powers of 4500 and 7000 Hz are comparable, which indicates that the spiral mode shapes of heat release can be the combining effects of those two frequencies.

The computed POD modes can be combined to reconstruct the responses of the 6L and PVC frequencies. Based on the discussions of mode shapes in Figs. 10 and 11, the 6L dominant longitudinal acoustic responses are reconstructed using modes 1 and 2 for the pressure and modes 1 and 4 for heat release; similarly, PVC dominant swirling responses are reconstructed using modes 10 and 11 for the pressure and modes 2 and 3 for the heat release.

The dominant reconstructed 6L response is shown in Fig. 12 and covers half of an acoustic cycle. From 0.14420 to 0.14454 s, the acoustic pressure at the chamber head goes from a compression to an expansion with a clear six half-wave mode in the chamber evident at times 1 and 2. During the intermediate period (times 2 and 3), diverse pressure mode shapes are present. At time 2, the amplitude of the pressure fluctuations is uniform throughout the chamber and air plenum, indicating a mean shift and a nonstationary behavior of the pressure oscillations. This can be further explained by the strong zero-frequency observed in PSD analysis of modes 1 and 2 temporal signals from Fig. 10. In addition, weaker contributions from the 5L

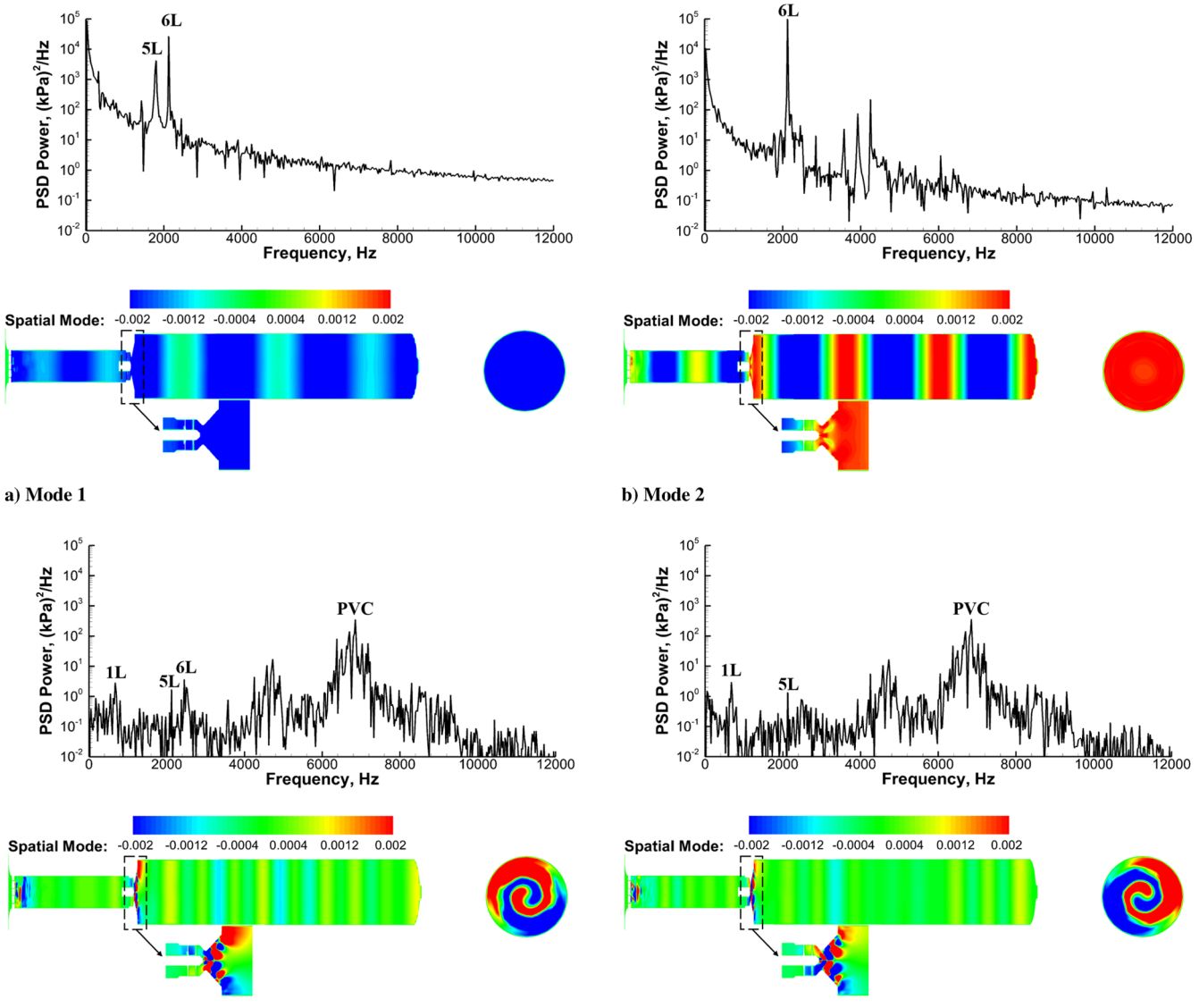

Fig. 10 Representative POD modes of pressure fluctuations in LDI combustor (the zoomed-in view is selected for the area highlighted by the dashed rectangular box, and the cross-section view of spatial mode is picked 1 mm downstream of the venturi).

acoustic mode can be identified at time 3, the frequency of which is found in POD mode 1 of the pressure.

Heat-release responses follow the pressure fluctuations and during the acoustic compression at the chamber head (time 1), and an increase in the heat release is observed in the diverging section with a decrease in the chamber. As discussed in [11,12], this is due to the strong acoustic forcing on the flowfield that brings more fuel upstream toward the venturi throat where the level of combustion is expected to rise. Going from acoustic compression to expansion (times 2 to 4), the heat release increases in the chamber while decreasing in the diverging section. This is attributed to the decrease in acoustic forcing at the chamber head, which allows for more fuel to enter chamber and react. Time 4 is the transition point from expansion to compression, the fuel is pushed back to the diverging section, and a local increase in heat release is observed therein.

The reconstructed PVC response is shown in Fig. 13 and covers a single cycle of swirling motion. A clockwise rotation can be inferred from the cross-sectional views of both pressure and heat-release responses, and a phase difference is observed by looking at the cross-section close to the venturi region. The heat release follows the high-pressure region in space and shows nonstationary amplitude changes. These changes are due to the weaker frequency peaks in modes 2 and 3 (Fig. 11). Moreover, as mentioned previously while discussing the pressure mode shapes, the presence of the longitudinal acoustic mode shapes is still identifiable in modes 10 and 11 in Fig. 10. It is difficult to disconnect the swirling motion from the longitudinal acoustic modes even though they have less power than the dominant PVC mode.

2. *DMD Analysis*

Unlike the POD analysis, the DMD technique provides decomposed modes at discrete frequencies. Figure 14 shows the DMD frequency spectrum. Both pressure and heat-release modes are shown. Pressure fluctuations show a spectrum that is similar to a standard PSD analysis (Figs. 2 and 4). Like with the POD, the nonstationary signal results in a zero-frequency mode. The benefit of DMD is that the DMD modes are organized in terms of a single frequency, unlike POD for which multiple frequencies are grouped together, making the individual impact of a single frequency impossible to discern. Heat-release fluctuations show a strong response to the 6L acoustic frequency and an additional excitation near the PVC frequency. This is similar to what is found in the POD analysis but is much more readily apparent.

The reconstructed pressure and heat-release responses for the 6L mode are shown in Fig. 15. The pressure response reconstructed from the DMD mode shows a global 6L acoustic mode shape. The heat release shows increased activity near the head end of the combustor with a complex mode shape around the venturi wall. The axial cut

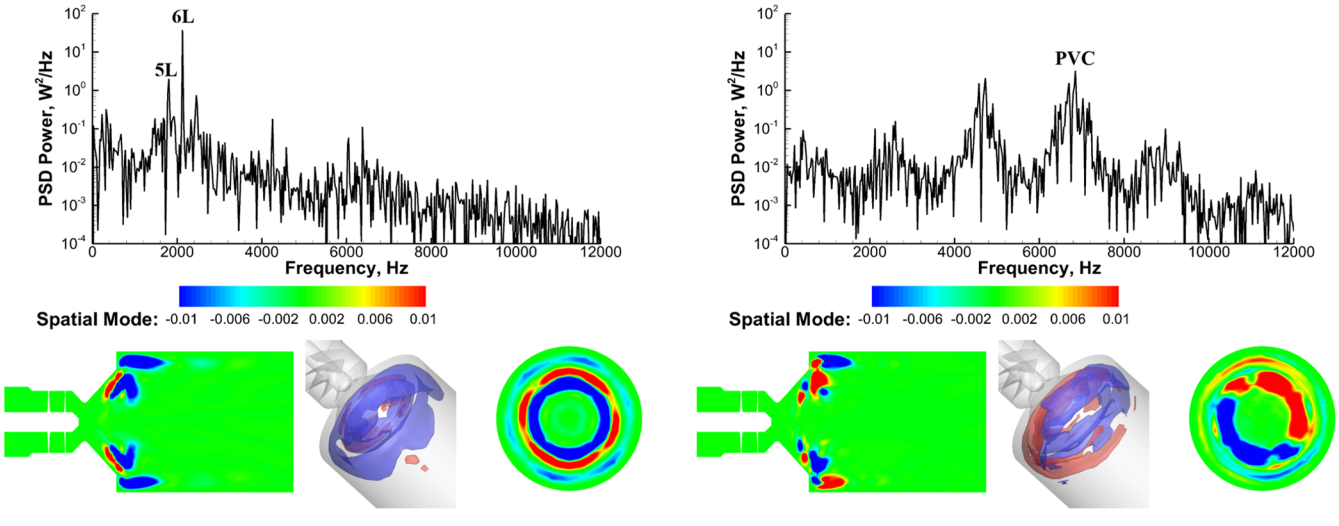

a) Mode 1

b) Mode 2

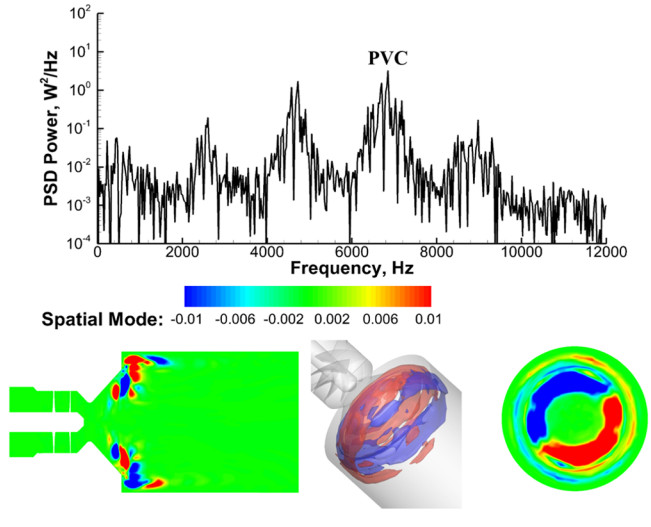

c) Mode 3

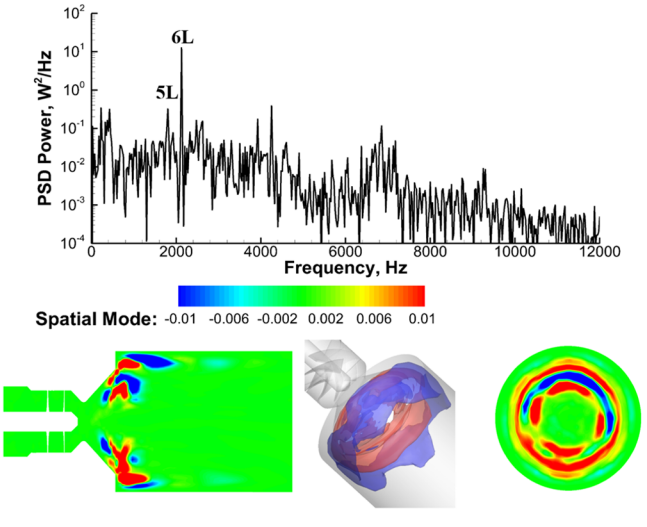

d) Mode 4

Fig. 11 Representative POD modes of heat-release fluctuations in LDI combustor (the three-dimensional view is shown with two representative isosurfaces corresponding to the minimum and maximum values in the contour legend, and the cross-section view of the spatial mode is picked 1 mm downstream of the venturi).

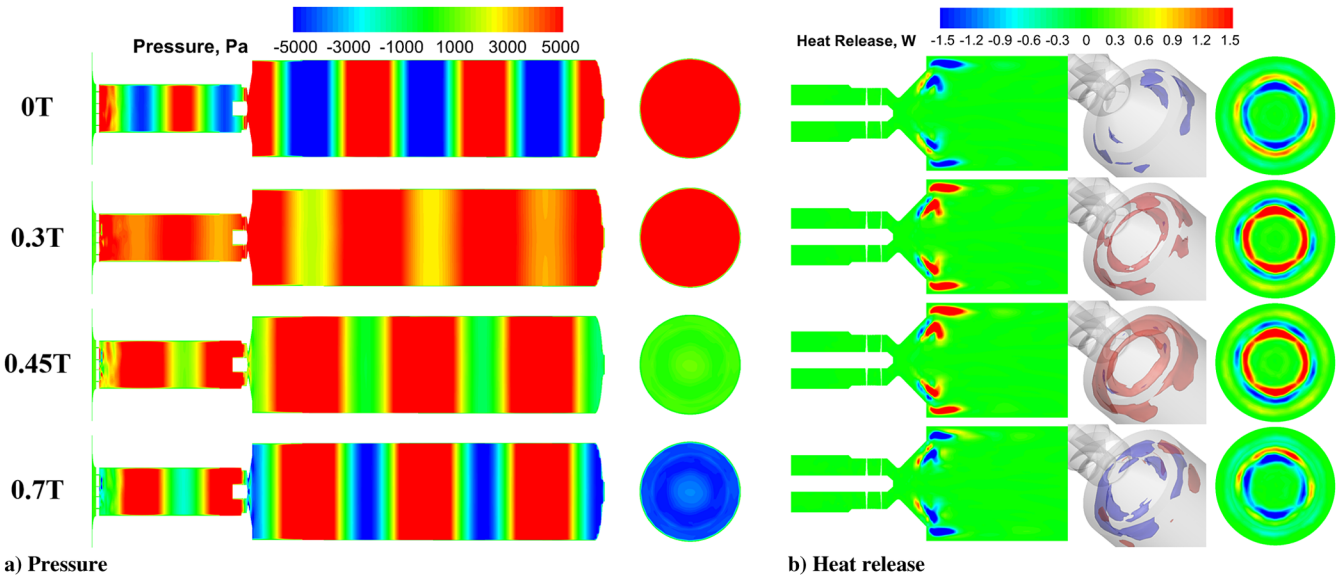

a) Pressure

b) Heat release

Fig. 12 Reconstructed 6L response of pressure and heat release using POD modes (modes 1 and 2 for pressure; modes 1 and 4 for heat release).

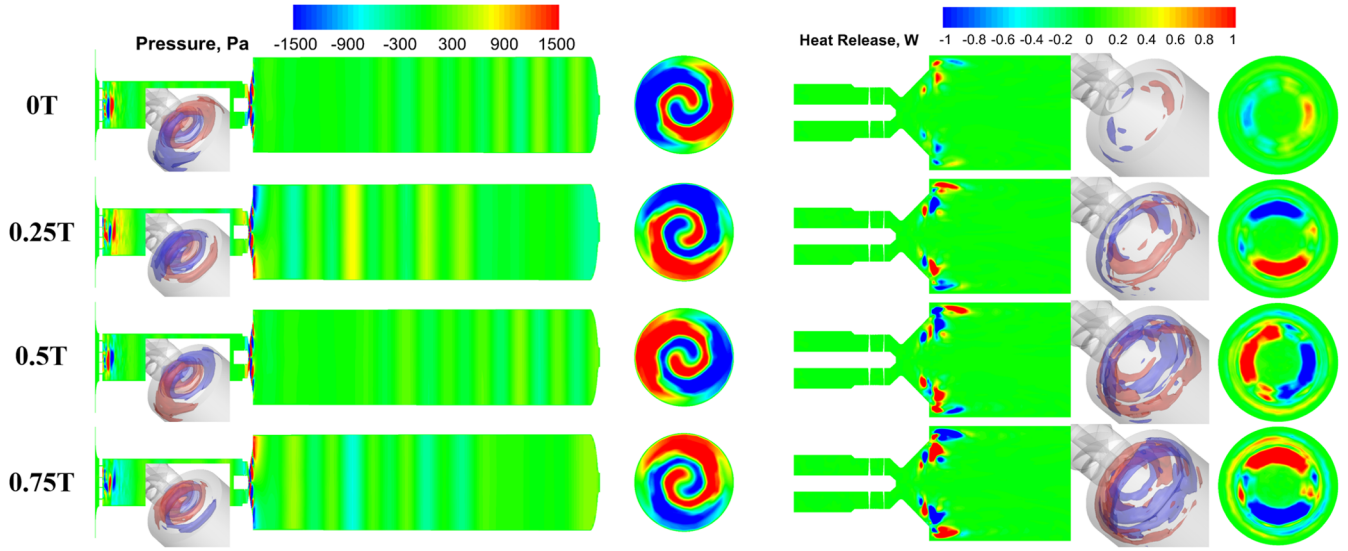

a) Pressure b) Heat release

Fig. 13 Reconstructed PVC response of pressure and heat release using POD modes (modes 10 and 11 for pressure; modes 2 and 3 for heat release).

shows that this complex mode shape is more or less axisymmetric, which is consistent with the fact that the 6L acoustic mode is a purely axial mode.

The PVC mode is shown in Fig. 16. A spiral structure is visible, which is similar to the mode shape from the POD decomposition shown in Fig. 13. The DMD decomposition shows that pressure fluctuations are restricted to the venturi section with very little response in the chamber, unlike the POD analysis (Fig. 13). This confirms that the PVC mode is due to the local swirling flow effects and the combustion taking place in that region.

For this single-element LDI gas turbine combustor, both POD and DMD analyses are able to capture the representative frequency responses found in Figs. 4 and 5. Two major responses are identified by both techniques. A strong longitudinally acoustic mode is present in the entire combustor, and a local swirl-driven PVC mode is present in the venturi section. POD provides spatial mode shapes corresponding to temporal evolutions that might contain a range of frequencies and cannot guarantee that there is a one-on-one correlation between different variables. It is difficult to associate specific physical phenomena with the POD modes directly. On the other hand, DMD generates decomposed modes sorted by frequency, providing a cleaner perspective of the different physical phenomena occurring at distinct frequencies. The response in different variables can be connected easily by comparing modes occurring at the same frequency. We conclude that DMD is therefore a more systematic and efficient tool for extracting and isolating physical phenomena from large data sets in which multiple physical phenomena are present.

B. Model Rocket Combustor (CVRC)

Comparisons between POD and DMD analyses is performed next by applying both techniques to the CVRC simulations. In this case, three different domains are used to assess the capabilities of both

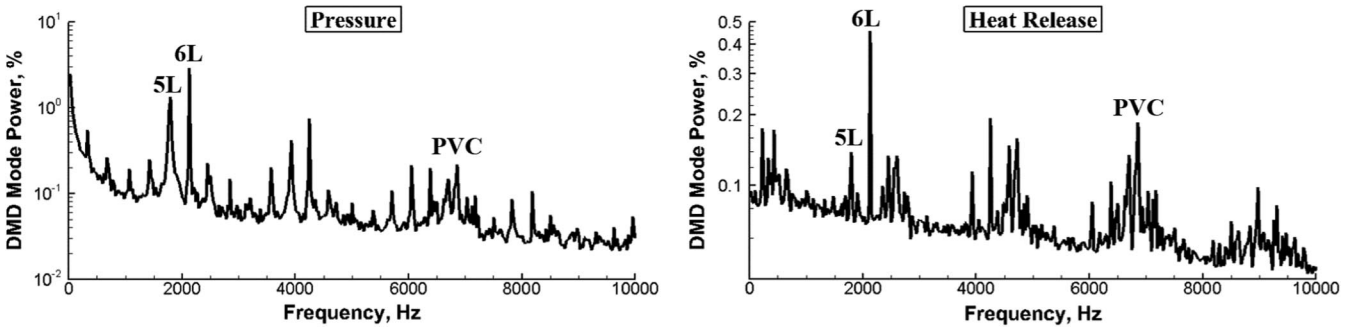

Fig. 14 DMD frequency spectrum for pressure (left) and heat-release (right) fluctuations in LDI combustor.

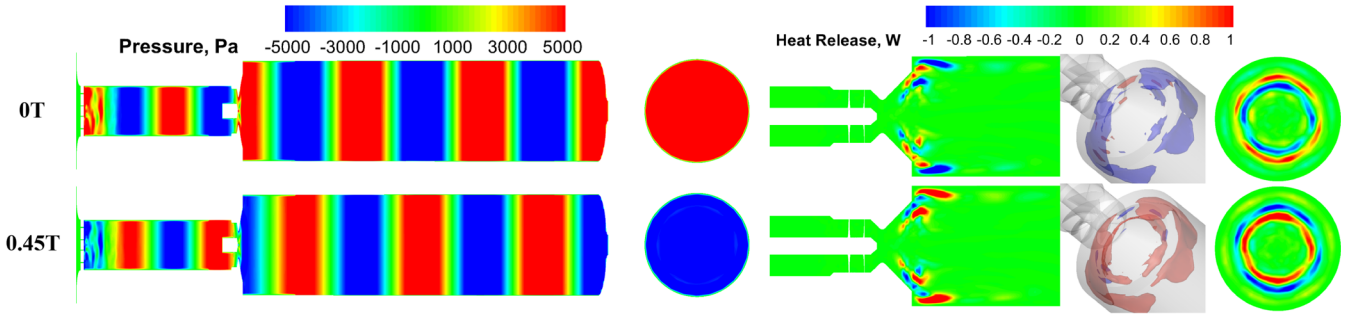

a) Pressure b) Heat Release

Fig. 15 DMD reconstruction of the 6L acoustic mode for pressure (left) and heat release (right) shown for two time instances.

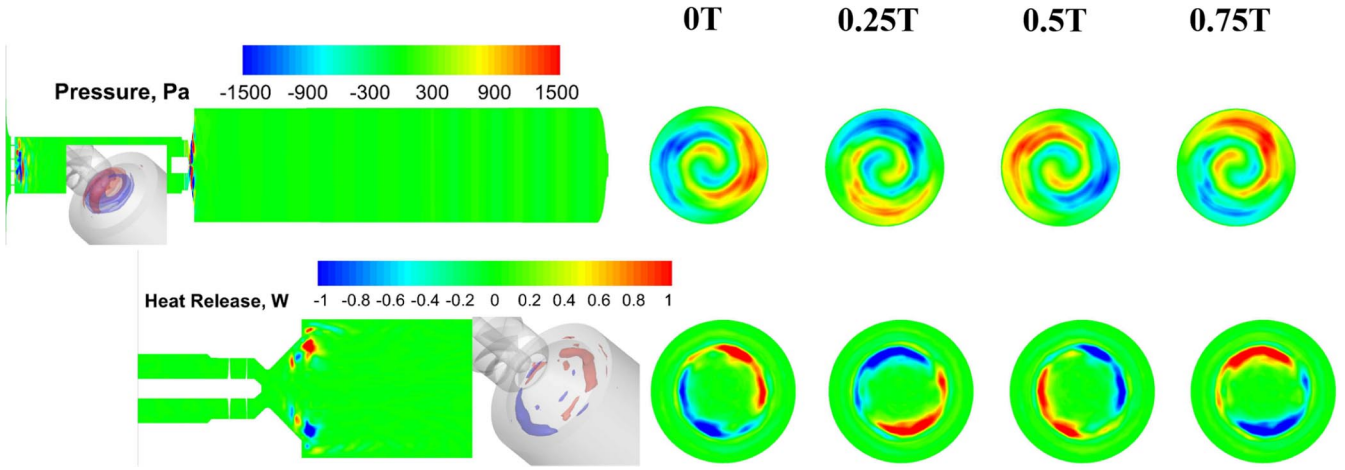

Fig. 16 DMD reconstruction of the PVC mode for pressure (top) and heat release (bottom).

techniques for treating data sets with incomplete information, which is often the case especially for experimental results. As shown in Fig. 6, domain I is the region where combustion takes place, only covering one-third of the chamber. The oxidizer post is absent resulting in incomplete information about the acoustics. Domain II is about one-fourth of the size of domain I and has incomplete information about both the combustion and acoustics. Along with domains I and II, the full domain is also be used to provide a baseline.

1. *POD Analysis*

The POD mode power and cumulative power for pressure and heat release are shown in Fig. 17 for the full domain and both subdomains. As in the LDI case, there is a rapid decrease in the pressure mode power while that of heat release is much flatter. With less acoustic response included in the analysis, domains I & II show sharper power distributions and faster power accumulation for the pressure than the full domain. However, there is little change in both the single and cumulative mode power distributions between the domains for the heat release.

The first two POD modes for pressure are shown in Fig. 18. The first POD mode of pressure shows both 1L and 2L acoustic frequencies in the PSD plot. The full domain shows a clear half-wave and half-wave configuration in both the chamber and post, which confirms the dominance of the 1L frequency in mode 1. The partial domains show reasonable agreement with the full domain for both the spatial and temporal component. Domain II shows higher PSD power at high frequencies (>6,000 Hz) than domain I and the full domain.

For the second mode, the spatial mode shape in the region spanning the partial domains is more complex than the first mode. This leads to very different and incorrect responses for the partial domains. Domains I and II have half-wave spatial modes that are correct for their domain size but incorrect for the global acoustics. The partial domains also show a discrepancy in the temporal signal content compared to the full domain. This indicates that extreme caution should be used when analyzing incomplete data sets.

The discrepancy in the POD analysis for the subdomains becomes even more apparent as the mode number increases. Figure 19 shows the spatial modes for modes 3 and 4. Domain I shows a full wave in mode 3 and nearly two full waves in mode 4. The 1T acoustic mode shows up in mode 3 of the domain II POD analysis, the frequency of which is around 13,000 Hz, and a twisted full wave configuration is seen in mode 4.

The first two POD modes of the heat-release fluctuations are shown in a similar manner with different domains in Fig. 20. POD analysis of full domain and domain I produces similar spatial mode shapes and frequency content in the PSDs of the temporal modes throughout the first four POD modes, which should be attributed to the fact that most of the combustion response is concentrated in domain I as highlighted in Fig. 6. Multiple frequencies are found in each POD mode, and the number of dominant frequencies increases as the POD mode number increases. POD modes 1 and 2 of domain II show similarities to the full domain and domain I results with the first five acoustic frequencies dominant in the temporal modes. A pulsing mode is identified in mode 1, which can be responsive to the strong driving force from the acoustic field as discussed in the cycle studies in [17]. Mode 2 has very similar frequency content as mode 1 but shows two alternative response spots of combustion in the spatial modes. For the higher POD modes (>2) of heat-release fluctuations, discrepancies between domains I and II and the full domain are more apparent, which is consistent with what has been observed in the pressure POD analysis as well.

By comparing the POD modes using different fractions of the domain, it has been shown that POD is sensitive to the completeness of the spatial information. The results and physical interpretations can be very different if an incomplete data set is used. This can be traced back to the fact that POD analysis decomposes modes to optimize the representations of the original data set, which can be compromised if some physical information is missing.

2. *DMD Analysis*

A DMD analysis is performed with the same domains that were used for the POD analysis. The DMD frequency spectra of pressure and heat-release fluctuations are shown in Fig. 21. Analysis of three domains shows consistency in terms of the frequencies picked up for

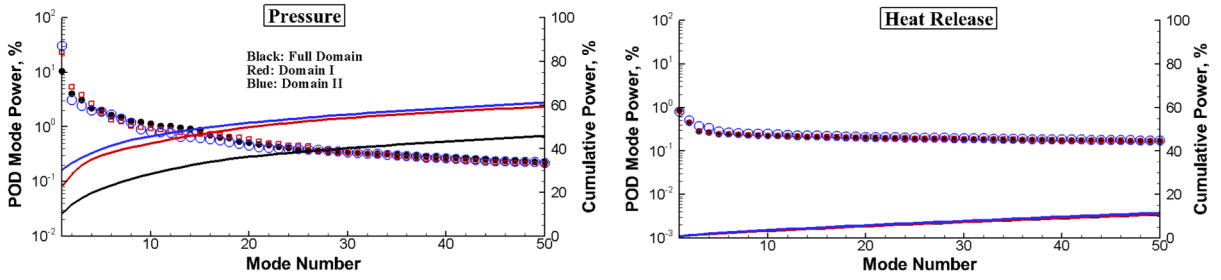

Fig. 17 POD mode power vs mode number for pressure (left) and heat-release (right) fluctuations in CVRC simulation with different domains (symbol: POD mode power; line: cumulative power).

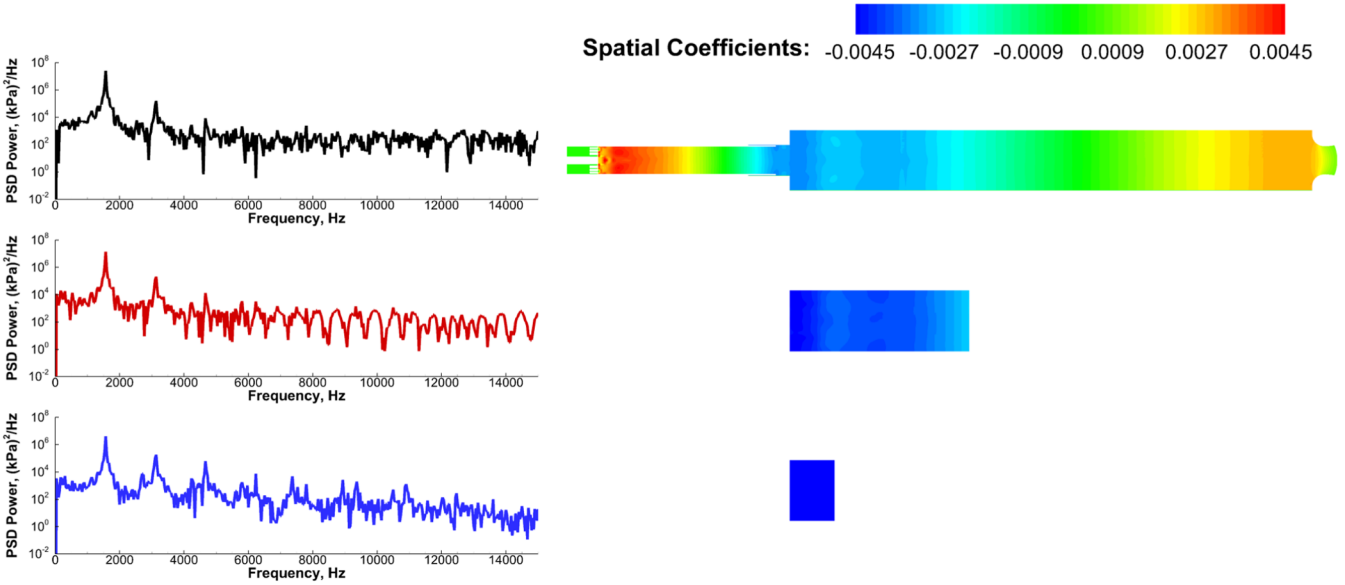

a) Mode 1

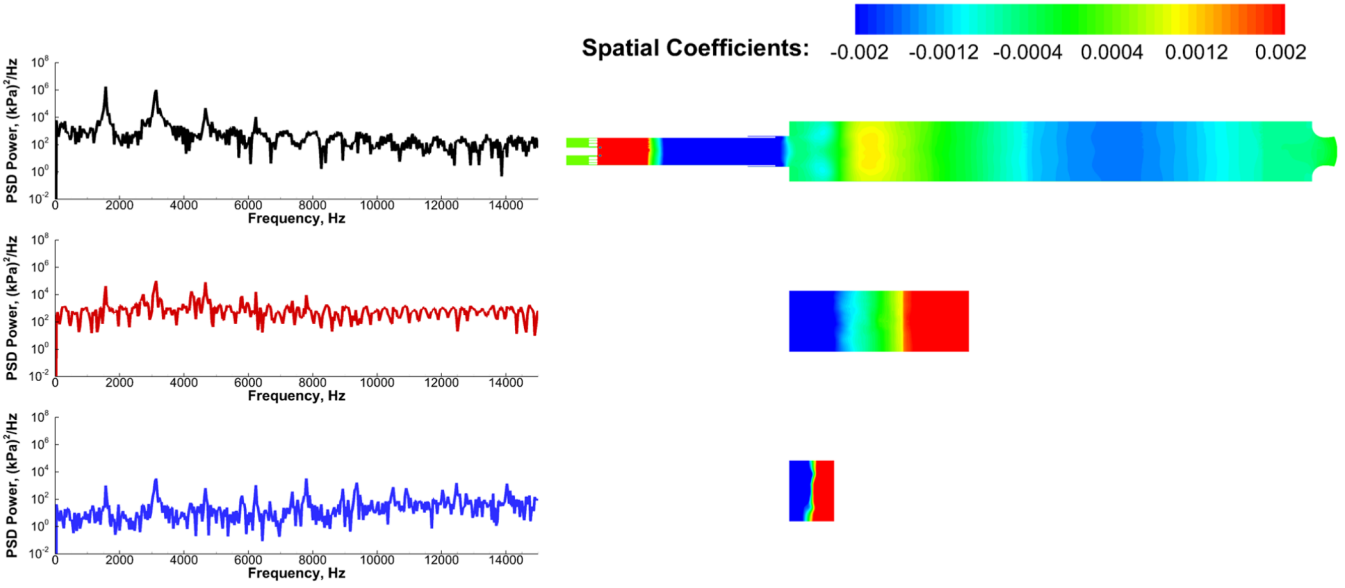

b) Mode 2

Fig. 18 POD modes 1 and 2 of pressure fluctuations in CVRC simulation.

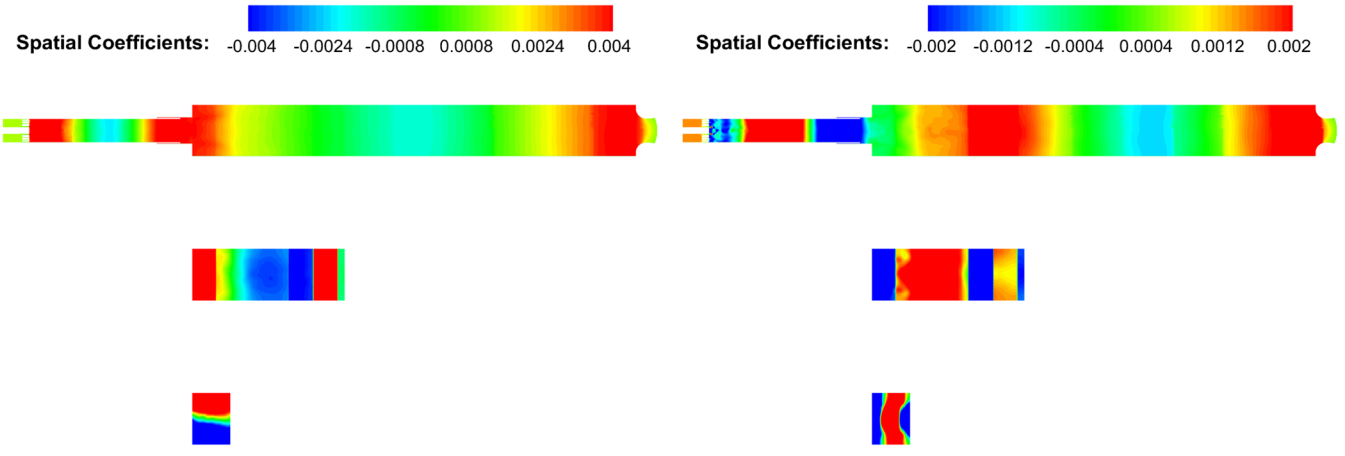

a) Mode 3 b) Mode 4

Fig. 19 POD modes 3 and 4 of pressure fluctuations for the three domains in the CVRC simulation.

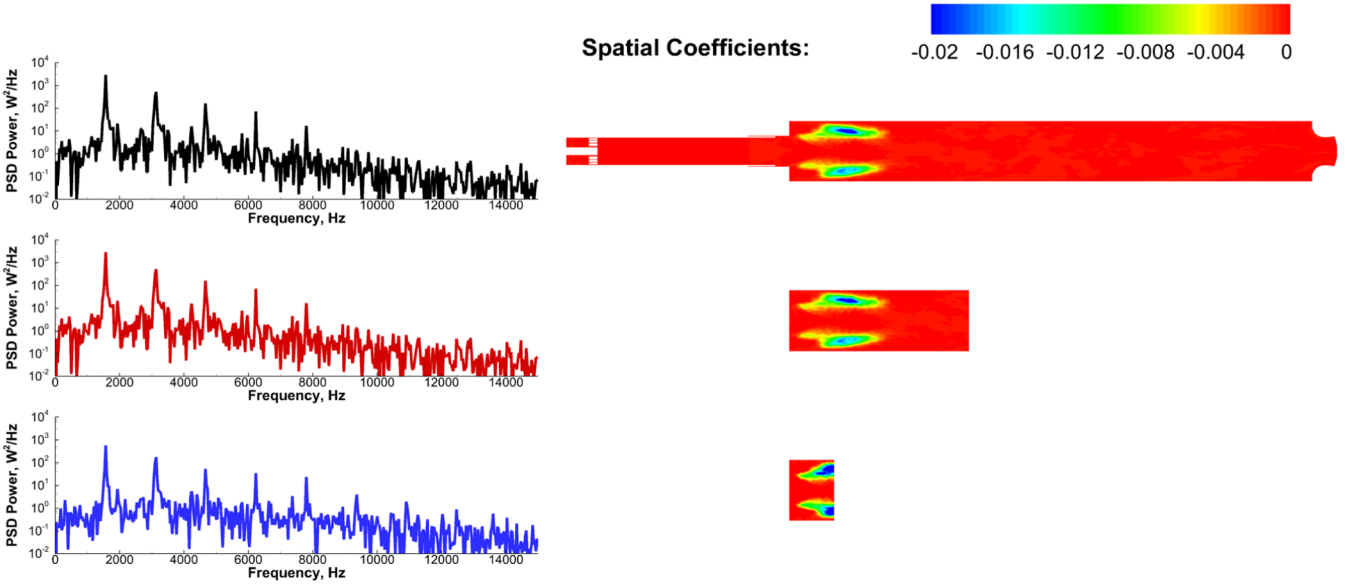

a) Mode 1

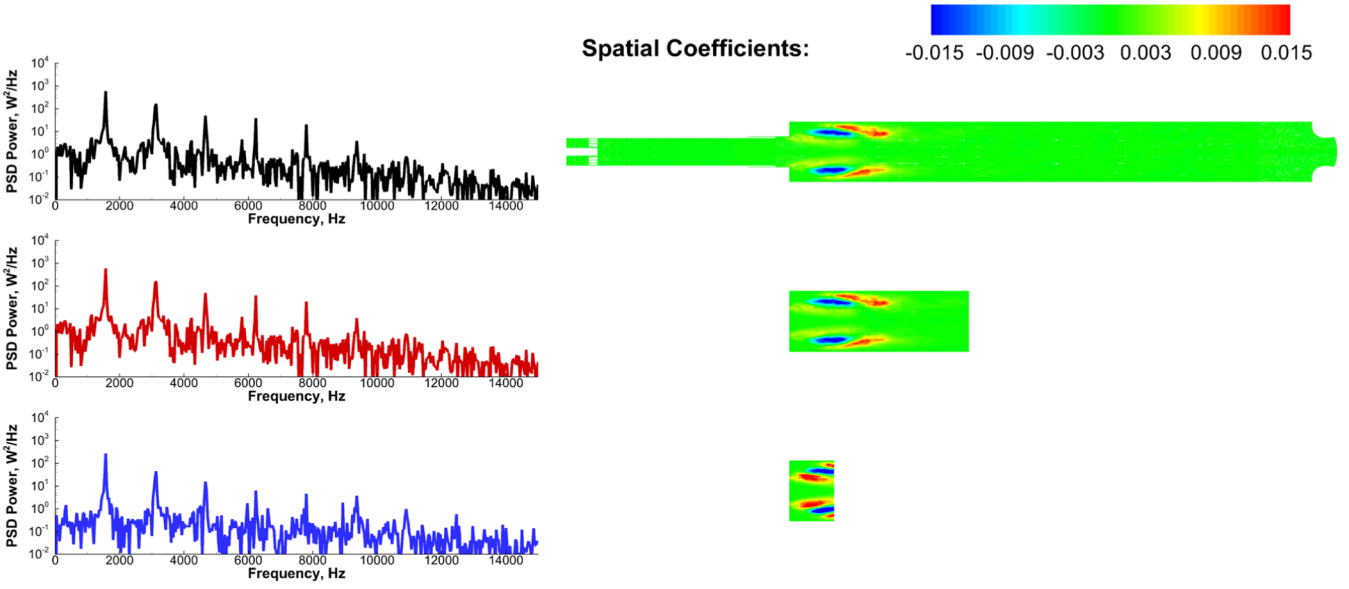

b) Mode 2

Fig. 20 POD modes 1 and 2 of heat-release fluctuations in the CVRC simulation.

both pressure and heat-release responses. Well-defined harmonic behavior can be found in the spectrum. Unlike what is found for the LDI case, the fundamental acoustic frequency (1L) is dominant here with a cascade of energy between the modes as the frequency increases. The heat release shows a harmonic response to the acoustic field.

The reconstructed responses at 1L frequencies are shown in Fig. 22. The responses corresponding to a full 1L cycle are selected to assess the capabilities of DMD analysis in capturing important dynamics when incomplete information is used. In both reconstructed 1L and 2L responses, DMD analysis of all three domains shows good consistency in terms of spatial distributions and temporal evolutions. More importantly, the relationship between the pressure and heat-release fluctuations is captured using each of the domains. From time 1 to 3 in Fig. 22, pressure rises at the chamber head section with an increase in heat release, and when it steps from time 3 to 4, the pressure drops in phase with the decrease in the heat release.

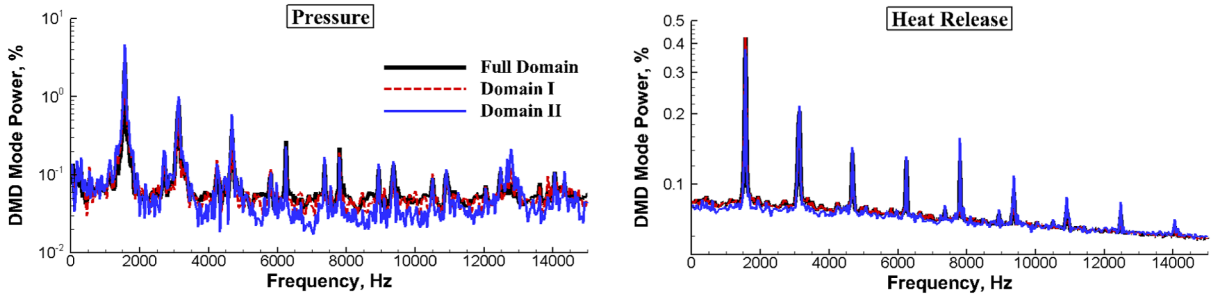

Fig. 21 DMD frequency spectrum for pressure (left) and heat-release (right) fluctuations in the CVRC simulation with different domains.

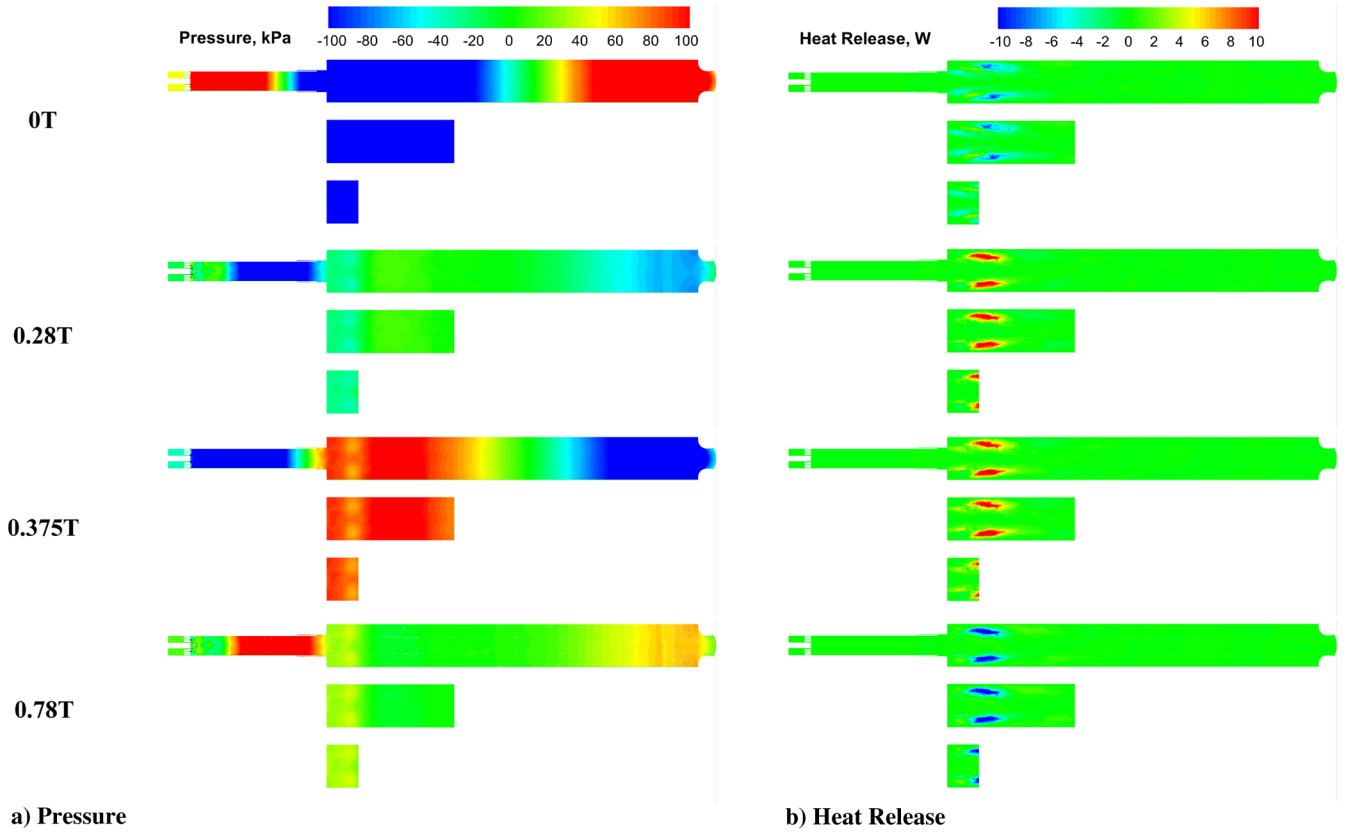

Fig. 22 Reconstructed 1L responses of pressure and heat release using DMD modes for the CVRC simulation.

Based on the application of the POD and DMD decomposition techniques on the simulation results of the LDI and CVRC configurations, the following conclusions can be drawn:

1) POD provides an optimized representation of the data set and captures the dominant responses efficiently; DMD provides modal decomposition based on frequency content.

2) Multiple frequencies are found in each POD mode. Frequencies of the dominant responses are present in lower modes, while weaker responses appear in higher modes. This makes it difficult to isolate the effect of different physical phenomena that occur at distinct frequencies. With DMD, a direct interpretation of dynamics occurring at discrete frequencies is produced.

3) POD modes of different quantities (e.g., pressure and heat release) are not directly correlated. DMD modes of different quantities can be easily correlated by comparing modes occurring at similar frequencies. The dynamics can be reconstructed accordingly to investigate possible physical coupling.

4) POD requires a complete set of spatial information to produce the correct modes. DMD can be used with partial sets of spatial information.

IV. Conclusions

This paper is concerned with the analysis of three-dimensional simulation results for self-excited combustion instabilities in a single-element lean direct injection (LDI) gas turbine combustor and a model rocket chamber, though the conclusions are applicable to a wide range of applications. Both proper orthogonal decomposition (POD) and dynamic mode decomposition (DMD) techniques are used as data-processing methods. It can be concluded from the LDI simulation results that the traditional bandpass-filtering technique is largely dependent on the results of a priori PSD analyses, which can be unreliable. Global longitudinal acoustic responses can be easily confirmed by checking several locations along the chamber, but there are high-frequency responses, which can be more difficult to pinpoint. In addition, by varying the parameters used for bandpass filtering (bandwidths and filter type), the signal amplitude and phases change.

Decomposition techniques provide a systematic approach to investigate important physics in complex systems. POD analysis provides a series of modes of decreasing energy content and an efficient and optimized way to represent the large data set. However, each mode corresponds to multiple frequencies. This makes it difficult to distinguish and isolate the specific contributions of phenomena that occur at distinct frequencies (as in the case of acoustics-driven combustion instabilities). There is no direct connection between the individual pressure and heat-release modes, making it difficult to make inferences about coupling (e.g., the precessing vortex core frequency is dominant in pressure POD modes 10 and 11 from Fig. 10 and in heat-release POD modes 3 and 4 from Fig. 11). One individual frequency can be spread over several nonneighboring POD modes (e.g., 5L frequency can be found in pressure POD modes 1, 10, and 11 as shown in Fig. 10). It was shown that the physical interpretations from POD can be variant to the completeness of spatial information included (e.g., the dominant chamber acoustic mode is not well captured using a fraction of the full domain as shown in Fig. 18). Using limited spatial information can provide poor results compared to the results using the entire spatial domain. For global phenomena like acoustics, the entire geometry is needed to ascertain the correct mode shapes. These factors limit the usefulness of POD for establishing correlations between multiple physical phenomena and analyzing cases with the recorded data not spanning the entire domain, which can be common for experiment measurement.

The frequency-based DMD technique provides modes that correspond to single frequencies. The global frequency spectrum can be obtained to help understand all the important periodic dynamics in the data set. Reponses at discrete frequencies can be simply investigated using DMD modes to get a clear picture of the dynamics (e, g., the reconstructed 6L responses using POD modes show evidence of other frequencies in Fig. 12, while cleaner mode shapes can be reconstructed using DMD modes in Fig. 15). Different physical processes (e.g., pressure and heat release) can be correlated in terms of frequencies to help postulate relevant mechanisms. Moreover, DMD analysis is able to provide consistent physical interpretations of the different spatial information given. As evaluated in Appendix B,

grid sensitivity studies show consistent results, but DMD results can be affected by temporal information, and to resolve certain desired response behavior, sufficient resolution is required. Therefore, DMD analysis proves to be a more systematic and useful tool than POD for studies of combustion instability.

Appendix A: Mathematical Model of Decomposition Techniques

The goal of decomposition is to approximate a function $z(x, t)$ over a specified domain as a finite sum of a temporal component $a_k(t)$ and a spatial component $\Phi_k(x)$,

$$z(x,t) \approx \sum_{k=1}^{N_p} a_k(t)\Phi_k(x) \tag{A1}$$

It is assumed that approximation becomes exact as N_p approaches infinity. Note that in Eq. (A1) there is no fundamental difference between x and t, but we usually think of x as a spatial coordinate and t as the temporal coordinate.

The representation of Eq. (A1) is not unique. For example, if the domain (either from experiment or computation) is a bounded interval $\boldsymbol{X}$ on the real line, then the functions $\Phi_k(x)$ can be chosen as a Fourier series, Legendre polynomials, Chebyshev polynomials, and so on. Different choices of the space-dependent function $\Phi_k(x)$ will result in different time-dependent functions $a_k(t)$. The time-dependent functions can be periodic or nonperiodic, single-frequency dominated, or multifrequency dominated.

In the POD analysis, the spatial functions $\Phi_k(x)$ are chosen to be orthonormal functions, i.e.,

$$\int_X \Phi_{k_1}(x)\Phi_{k_2}(x)\,\mathrm{d}x = \begin{cases} 1 & \text{if } k_1 = k_2 \\ 0 & \text{otherwise} \end{cases} \tag{A2}$$

The orthonormality of Φ_k means that a_k can be determined using only Φ_k, as opposed to all of the Φ functions,

$$a_k(t) = \int_X z(x,t)\Phi_k(x)\,\mathrm{d}x \tag{A3}$$

A1. Singular Value Decomposition in POD Analysis

In practice, whole data sets or snapshots are arranged into a POD matrix first, for example, with each row containing the temporal data and each column containing the spatial data. Thus, if there are N rows of temporal data and m columns of spatial data, the POD matrix will be of size $N \times m$.

Once we obtain the POD matrix A, the SVD of A is

$$A = U\Sigma V^T \tag{A4}$$

where U is an $N \times N$ orthogonal matrix, V is an $m \times m$ orthogonal matrix, and Σ is an $N \times m$ matrix with all elements zero except along the diagonal. The diagonal elements of Σ consist of $N_p = \min(N, m)$ nonnegative numbers σ_i, which are the singular values of A. The singular values are unique and are arranged in decreasing magnitude,

$$\sigma_i > \sigma_{i+1} \tag{A5}$$

In Eq. (A5), let $Q = U\Sigma$. Then, $A = QV^T$. Letting $\boldsymbol{q}_k$ be the kth column of Q and $\boldsymbol{v}_k$ be the kth column of V, we write out the matrix product as

$$A = QV^T = \sum_{k=1}^{N_p} \boldsymbol{q}_k \boldsymbol{v}_k^T \tag{A6}$$

Equation (A6) is the discrete form of Eq. (A1). The matrix for each POD mode is

$$A_k = \boldsymbol{q}_k \boldsymbol{v}_k^T \tag{A7}$$

In Eq. (A7), A_k is defined as the kth POD mode for matrix A, and it is noted that A_k has the same dimensions as the matrix A. Moreover, the column matrix $\boldsymbol{q}_k$ can be interpreted as the temporal mode of the kth POD mode, while the column matrix $\boldsymbol{v}_k$ represents the spatial mode. If the temporal mode $\boldsymbol{q}_k$ is obtained such that $Q = U\Sigma$, the spatial mode $\boldsymbol{v}_k$ contains all normalized numbers and vice versa. Or we can write Eq. (A7) in this way:

$$A_k = \boldsymbol{u}_k \sigma_k \boldsymbol{v}_k^T \tag{A8}$$

In Eq. (A8), $\boldsymbol{u}_k$ is the kth column of U, and σ_k corresponds to the kth singular value of matrix A. The σ_k is defined as the mode power of the kth POD mode, and it indicates mathematically how representative the decomposed modes are compared with raw data, and physically it represents the level of information that one can extract in terms of the decomposed modes from the original data.

A2. Arnoldi Algorithm in DMD Analysis

DMD analysis decomposes the data by frequency. To obtain single frequency dynamic modes, suppose the data set is represented as a sequence of snapshots,

$$V_1^N = \{\boldsymbol{v}_1, \boldsymbol{v}_2, \boldsymbol{v}_3, \ldots, \boldsymbol{v}_N\} \tag{A9}$$

where $\boldsymbol{v}_i$ stands for the ith snapshot of the data. DMD assumes that a linear map exists between a snapshot and the next snapshot in the sequence; thus, if B represents the linear map, $\boldsymbol{v}_{i+1} = B\boldsymbol{v}_i$. Therefore,

$$V_1^N = \{\boldsymbol{v}_1, B\boldsymbol{v}_1, B^2\boldsymbol{v}_1, \ldots\ldots, B^{N-1}\boldsymbol{v}_1\} \tag{A10}$$

Another assumption is that there exists a specific number N, beyond which the vector $\boldsymbol{v}_N$ can be expressed as linear combination of the previous vectors,

$$\boldsymbol{v}_N = a_1\boldsymbol{v}_1 + a_2\boldsymbol{v}_2 + \cdots + a_{N-1}\boldsymbol{v}_{N-1} \text{ or } \boldsymbol{v}_1 = V_1^{N-1}\boldsymbol{a} + \boldsymbol{r} \tag{A11}$$

Hence,

$$BV_1^{N-1} = V_2^N = V_1^{N-1}S + re_{N-1}^T \tag{A12}$$

where

$$S = \begin{pmatrix} 0 & & & & a_1 \\ 1 & 0 & & & a_2 \\ & \ddots & \ddots & & \vdots \\ & & 1 & 0 & a_{N-2} \\ & & & 1 & a_{N-1} \end{pmatrix} \tag{A13}$$

Applying the eigenvalue decomposition for matrix S,

$$S = T\Lambda T^{-1} \tag{A14}$$

where matrix T is the eigenvector matrix of S. If a sufficient number of snapshots is used, the eigenvalues of S are representative of the eigenvalues of B, which contain the time-evolution information of the flowfield.

Similarly the kth dynamic mode corresponding to the frequency response can be constructed as

$$\boldsymbol{\Psi}_k = V_1^{N-1}\boldsymbol{y}_k \tag{A15}$$

where $\boldsymbol{y}_k$ is the kth eigenvector of matrix S in Eq. (A14). The original data set can be decomposed into the form in Eq. (A1),

$$V_1^{N-1} = \sum_k \boldsymbol{\Psi}_k \boldsymbol{y}_k^T \tag{A16}$$

where $\mathbf{\Psi}_k$ contains the dynamic spatial information and $\boldsymbol{y}_k$ contains the temporal evolutional information.

A3. Practical Implementations of DMD Analysis

As pointed out by Schmid [21], even though the previous Arnoldi algorithm is mathematically correct, in practical implementations, the companion matrix S can be ill conditioned, especially when the data are contaminated with noise. Therefore, a more robust implementation is used for DMD analysis in the current studies. First, the snapshots are arranged as in Eq. (A9) to get matrix V_1^N and apply a SVD,

$$V_1^N = W\Sigma U^T \tag{A17}$$

where matrices W and U are both orthonormal and contain spatial and temporal information, respectively. Substitute Eqs. (A17) into (A12):

$$\begin{aligned} &BW\Sigma U^T = V_2^N \\ &\Rightarrow BW = V_2^N U\Sigma^{-1} \\ &\Rightarrow W^T BW = W^T V_2^N U\Sigma^{-1} = \tilde{S} \end{aligned} \tag{A18}$$

It should also be noted from Eq. (A12) that $V_2^N \approx V_1^{N-1}S$, so

$$\begin{aligned} &W^T V_1^{N-1} SU\Sigma^{-1} = \tilde{S} \\ &\Rightarrow W^T(W\Sigma U^T)SU\Sigma^{-1} = \tilde{S} \\ &\Rightarrow (\Sigma U^T)S(\Sigma U^T)^{-1} = \tilde{S} \end{aligned} \tag{A19}$$

And it can be seen that $\tilde{S}$ is a similarity matrix to S and they share the same eigenvalues. Therefore, eigenvalue decomposition is applied to $\tilde{S}$ instead of S,

$$\tilde{S} = \tilde{T}\,\tilde{\Lambda}\,\tilde{T}^{-1} \tag{A20}$$

In that way, the kth spatial mode can be calculated as

$$\mathbf{\Psi}_k = W\tilde{\boldsymbol{y}}_k \tag{A21}$$

where $\tilde{\boldsymbol{y}}_k$ is the kth eigenvector of matrix $\tilde{S}$ in Eq. (A20) and the temporal modes can be computed as

$$\boldsymbol{y}_k = U\Sigma^{-1}\tilde{\boldsymbol{y}}_k \tag{A22}$$

Each DMD mode corresponds to a single frequency f_k,

$$2\pi f_k = \log(\mu_{k,i})/\Delta t \tag{A23}$$

where $\mu_{k,i}$ is the imaginary of the kth eigenvalue of matrix $\tilde{S}$ in Eq. (A20) and Δt is the time step in between two snapshots. Unlike POD, which produces modes in all real numbers, DMD modes consist of complex numbers, and usually each individual frequency is related to two modes, complex conjugate to each other. Therefore, the responses V_k corresponding to the kth frequency can be reconstructed by taking the real part of DMD spatial and temporal modes' product,

$$V_k = Re\{\mathbf{\Psi}_k \boldsymbol{y}_k^T\} \tag{A24}$$

Appendix B: Performance Evaluation of Dynamic Mode Decomposition

From the discussions in Sec. III, DMD is better suited to investigating the effects of multiple physical phenomena occurring simultaneously. In this section, the DMD analysis is further examined by using different time intervals and computational grids to investigate the influence of data quality on the results.

Table B1 Testing temporal quality information

Case name	Time interval	Sample rate, kHz	Number of 1L cycles	Number of 6L cycles	Δf, Hz
Interval I	$0.12 \sim 0.14$ s	100	6	36	50
Interval II	$0.12 \sim 0.15$ s	100	10	60	33
Interval III	$0.12 \sim 0.16$ s	100	13	78	25

B1. Sensitivity Study of Temporal Quality

The LDI simulation is used in this section to evaluate the sensitivity of DMD to the amount of quasi-periodic dynamics included in the analysis. Three different time intervals are used for the studies, the summary of which can be found in Table B1. The sample rate is kept the same to guarantee the range of frequencies that can be captured in the analysis. Results presented earlier use the most information (interval III), and intervals I and II contain less temporal information then Interval III.

The DMD frequency spectrum for the three time intervals is shown in Fig. B1. As the time interval is decreased, frequency resolution decreases, and this broadens the bands and makes the frequency peaks less definite. The low-frequency responses can be important because it has been postulated that couplings between higher harmonic hydrodynamic instabilities and acoustic modes are the driving mechanisms that sustain combustion instability in the single-element LDI combustor and the fundamental frequencies happen to lie in the low-frequency region highlighted previously [11,12].

The effects of time interval lengths are studied by comparing the reconstructed responses at the 1L frequency for both pressure and heat-release fluctuations shown in Fig. B2. Comparisons are performed in terms of the response during the acoustic compression phase at the head section. Pressure modes from the different time-interval lengths show a well-defined half-wave mode shape in the combustor, and correspondingly, the heat-release modes indicate growth during the acoustic compression. Although the DMD analysis gives consistent pressure response and correlations between pressure and heat release, differences in the heat-release mode shapes are still identifiable. With the longer time interval, the dynamics of heat release becomes less noisy than the ones with a shorter interval. There are fewer heat-release decaying spots during acoustic compression and fewer growing spots during acoustic expansions. So, it seems that when more temporal information is included in the analysis, the reconstructed responses are more definite, and the coupling between the different physics is easier to identify. Of course, this also means the investment of more computational resources for the analysis.

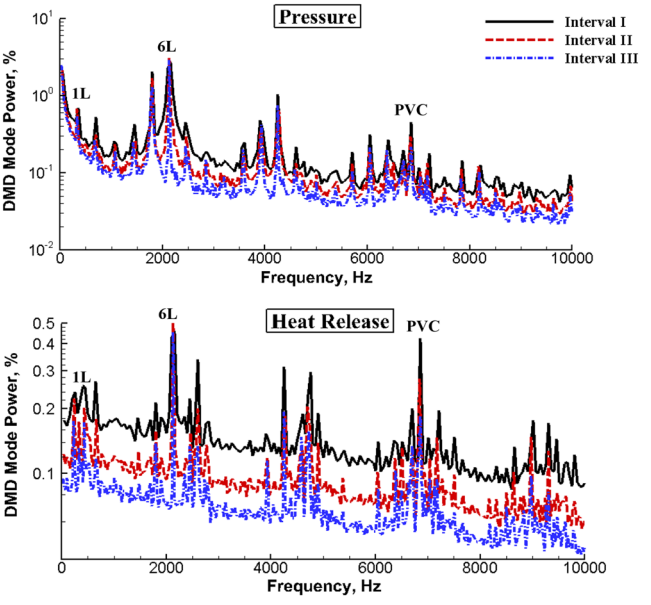

Fig. B1 DMD frequency spectrum for heat-release fluctuations in LDI combustor simulation using different time intervals.

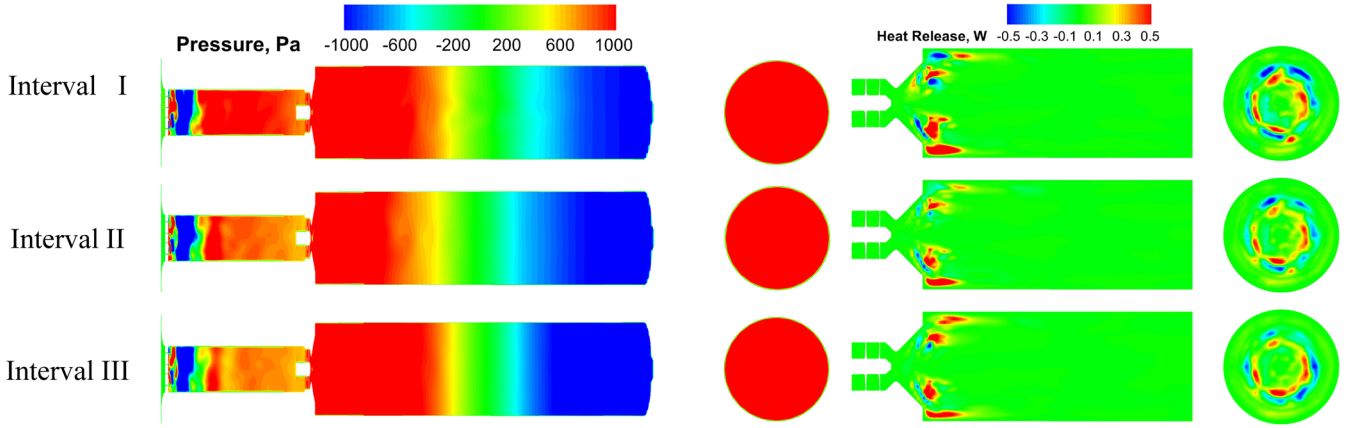

Fig. B2 Reconstructed 1L responses of pressure (left) and heat release (right) using DMD modes for LDI simulation using different time intervals.

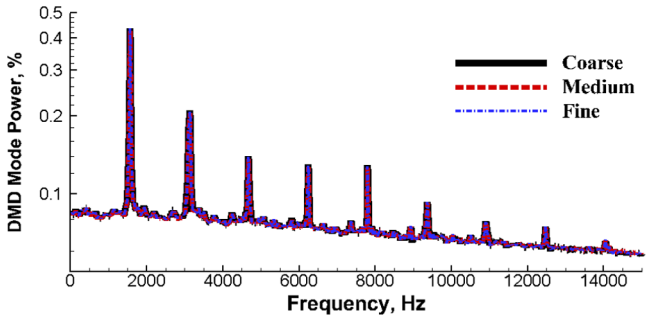

Fig. B3 DMD frequency spectrum for heat-release fluctuations in the CVRC simulation using different sets of grids.

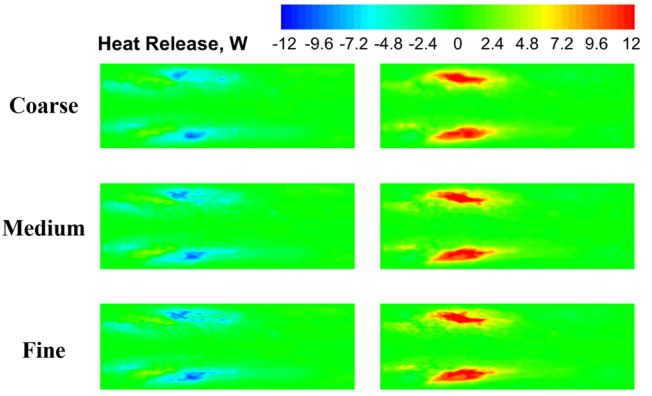

Fig. B4 Reconstructed 1L responses of pressure and heat release using DMD modes for the CVRC simulation using different sets of grids.

B2. Sensitivity Study of Grid Resolution

The CVRC simulation is next used as the test case to examine the sensitivity of DMD analysis to grid resolution. Only heat-release fluctuations in the combustion zone (domain I shown in Fig. 6) are used for this study. Grid points in the azimuthal direction are kept the same due to the longitudinal nature of the physics observed in both the experiments [18] and simulations [17], and the refinement of grids is performed in three levels as summarized in Table B2. Also, it should be noted that the medium grid is the same as that used for the results in Sec. III.B.

The DMD frequency spectrum of the heat-release fluctuations is shown in Fig. B3 for the three different grid resolutions, and the dominant frequency peaks are captured consistently by the DMD analysis.

The reconstructed responses at the 1L frequency with different grid resolutions are shown in Fig. B4. The response during acoustic expansion and compression are shown here for comparisons, which correspond to times 1 and 3 in Fig. 22. Differences in the 1L responses are very small, and the DMD results are able to capture consistent spatial distributions and temporal evolutions for the heat-release variations.

The DMD 2L response shows more differences in the spatial distribution, but it is still capable of describing the dominant dynamics of interest. Small improvements can be observed in the top half of the domain with the grid refinement.

Table B2 Testing grid information

	Domain I		
Case Name	x	R	θ
Coarse	60	12	24
Medium	120	24	24
Fine	200	48	24

Based on the temporal quality and grid sensitivity studies for the DMD analysis, it can be concluded that with sufficiently resolved information input the DMD analysis provides a consistent mode shape and is capable of extracting the dynamics at discrete frequencies reliably.

Here, the information input includes 1) sufficient grid points to resolve the physics of interests (i.e., combustion and acoustics) and 2) a sufficient number of repeatable quasi-periodic information to resolve the dynamic response of interest (e.g., the longitudinal acoustic-driven combustion response).

Acknowledgments

The authors acknowledge the support of NASA under grant number NNX11AI62A, with Program Manager Julie Fowler and Technical Monitor Kevin Breisacher, and NCC3-989, with Program Manager Claudia Meyer. The authors would like to acknowledge financial support from John Zink Company. Also, the authors wish to acknowledge the technical advice of Charles Merkle and the recommendations regarding dynamic mode decomposition from Sébastien Ducruix of Laboratoire EM2C at Ecole Centrale, Paris.

References

[1] Shi, L. L., Liu, Y. Z., and Wan, J. J., "Influence of Wall Proximity on Characteristics of Wake Behind a Square Cylinder: PIV Measurements and POD Analysis," *Experimental Thermal and Fluid Science*, Vol. 34, No. 1, 2010, pp. 28–36. doi:10.1016/j.expthermflusci.2009.08.008

[2] Bouhoubeiny, E., and Druault, P., "Note on the POD-Based Time Interpolation from Successive PIV Images," *Comptes Rendus Mécanique*, Vol. 337, Nos. 11–12, 2009, pp. 776–780. doi:10.1016/j.crme.2009.10.003

[3] Berkooz, G., Holmes, P., and Lumley, J. L., "The Proper Orthogonal Decomposition in the Analysis of Turbulent Flows," *Annual Review of Fluid Mechanics*, Vol. 25, 1993, pp. 539–575. doi:10.1146/annurev.fl.25.010193.002543

[4] Iudiciani, P., Duwig, C., Husseini, S. M., Szasz, R. Z., Fuchs, L., and Gutmark, E. J., "Proper Orthogonal Decomposition for Experimental Investigation of Flame Instabilities," *AIAA Journal*, Vol. 50, No. 9, 2012, pp. 1843–1854. doi:10.2514/1.J051297

[5] Huang, Y., Wang, S., and Yang, V., "Systematic Analysis of Lean-Premixed Swirl-Stabilized Combustion," *AIAA Journal*, Vol. 44, No. 4, 2006, pp. 714–740. doi:10.2514/1.15382

[6] Zong, N., and Yang, V., "Supercritical Fluid Dynamics of Pressure Swirl Injector with External Excitations," *43rd AIAA/ASME/SAE/ASEE Joint Propulsion Conference and Exhibit*, AIAA Paper 2007-5458, 2007.

[7] Seena, A., and Sung, H. J., "Dynamic Mode Decomposition of Turbulent Cavity Flows for Self-Sustained Oscillations," *International Journal of Heat and Fluid Flow*, Vol. 32, No. 6, 2011, pp. 1098–1110. doi:10.1016/j.ijheatfluidflow.2011.09.008

[8] Muld, T. W., Efraimsson, G., and Henningson, D. S., "Flow Structures Around a High-Speed Train Extracted Using Proper Orthogonal Decomposition and Dynamic Mode Decomposition," *Computers and Fluids*, Vol. 57, No. 30, 2012, pp. 87–97. doi:10.1016/j.compfluid.2011.12.012

[9] Kalghatgi, P., and Acharya, S., "Modal Analysis of Countercurrent Shear Flows," *42nd AIAA Fluid Dynamics Conference and Exhibit*, AIAA Paper 2012-3080, 2012.

[10] Motheau, E., Nicoud, F., and Poinsot, T., "Mixed Acoustic–Entropy Combustion Instabilities in Gas Turbines," *Journal of Fluid Mechanics*, Vol. 749, 2014, pp. 542–576. doi:10.1017/jfm.2014.245

[11] Huang, C., Yonnc, C., Gejji, R., Anderson, W., and Sankaran, V., "Computational Study of Combustion Dynamics in a Single-Element Lean Direct Injection Gas Turbine Combustor," *52nd Aerospace Sciences Meeting*, AIAA Paper 2014-0620, 2014.

[12] Huang, C., Gejji, R., Anderson, W., Yonnc, C., and Sankaran, V., "Combustion Dynamics Behavior in a Single-Element Lean Direct Injection (LDI) Gas Turbine Combustor," *50th AIAA/ASME/SAE/ASEE Joint Propulsion Conference*, AIAA, Paper 2014-3433, 2014.

[13] Gejji, R., Cheng, H., Yonnc, C., and William, A., "A Parametric Study of Combustion Dynamics in a Single-Element Lean Direct Injection Gas Turbine Combustor: Part II: Experimental Investigation," *52nd Aerospace Sciences Meeting*, AIAA, Paper 2014-0133, 2014.

[14] Harvazinski, M., Xia, G., Anderson, W., and Merkle, C., "Analysis of Self-Excited Combustion Instability Using a Combination of Two- and Three-Dimensional Simulations," *50th AIAA Aerospace Sciences Meeting including the New Horizons Forum and Aerospace Exposition*, AIAA Paper 2012-0782, 2012.

[15] Harvazinski, M., "Modeling Self-Excited Combustion Instabilities Using a Combination of Two- and Three-Dimensional Simulations," Ph. D. Thesis, Purdue Univ., West Lafayette, IN, 2012.

[16] Garby, R., Selle, L., and Poinsot, T., "Large-Eddy Simulation of Combustion Instabilities in a Variable-Length Combustor," *Comptes Rendus Mécanique*, Vol. 341, Nos. 1–2, 2013, pp. 220–229. doi:10.1016/j.crme.2012.10.020

[17] Harvazinski, M. E., Huang, C., Sankaran, V., Feldman, T. W., Anderson, W. E., Merkle, C. L., and Talley, D. G., "Coupling Between Hydrodynamics, Acoustics, and Heat Release in a Self-Excited Unstable Combustor," *Physics of Fluids*, Vol. 27, No. 4, 2015, pp. 1–27. doi:10.1063/1.4916673

[18] Feldman, T., Harvazinski, M., Merkle, C., and Anderson, W., "Comparison Between Simulation and Measurement of Self-Excited Combustion Instability," *48th AIAA/ASME/SAE/ASEE Joint Propulsion Conference & Exhibit*, AIAA Paper 2012-4088, 2012.

[19] Chatterjee, A., "An Introduction to the Proper Orthogonal Decomposition," *Current Science*, Vol. 78, 2000, pp. 808–817.

[20] Rowley, C. W., MeziĆ, I., Bagheri, S., Schlatter, P., and Henningson, D. S., "Spectral Analysis of Nonlinear Flows," *Journal of Fluid Mechanics*, Vol. 641, 2009, pp. 115–127. doi:10.1017/S0022112009992059

[21] Schmid, P. J., "Dynamic Mode Decomposition of Numerical and Experimental Data," *Journal of Fluid Mechanics*, Vol. 656, 2010, pp. 5–28. doi:10.1017/S0022112010001217

[22] Sayadi, T., Nichols, J. W., Schmid, P. J., and Jovanovi´, M. R., "Dynamic Mode Decomposition of H-type Transition to Turbulence," *Proceedings of the Summer Program*, Center for Turbulence Research, 2012, pp. 5–14.

J. P. Drummond
Associate Editor